Highly Stable Fe/Co-TPY-MIL-88(NH2) Metal-Organic Framework (MOF) in

Enzymatic Cascade Reactions for Chemiluminescence-based Detection of Extracellular

Vesicles

Qiaoshi Jiang, Yuchen Xiao, Anh N. Hong, Yuyang Shen, Zongbo Li, Pingyun Feng<sup>2,\*</sup> and Wenwan

Zhong<sup>1, 2, \*</sup>

<sup>1</sup>Environmental Toxicology Graduate Program; <sup>2</sup>Department of Chemistry, University of

California-Riverside, Riverside, CA 92521, U.S.A.

\* Corresponding author

Pingyun Feng, email: pingyun.feng@ucr.edu

Wenwan Zhong, email: wenwan.zhong@ucr.edu

KEYWORDS: Metal-organic Frameworks; Pore partition agent; Nanozymes; Peroxidase-like

Activity; Enzymatic Cascade Reaction; Chemiluminescence; Extracellular Vesicles.

## Abstract

Metal-Organic Frameworks (MOFs) can deliver many advantages when acting as enzyme mimics to assist with signal amplification in molecular detection: they have abundant active catalytic sites per unit volume of the material; their structures and elemental compositions are highly tunable, and their high specific surface area and porous property can assist with target separation and enrichment. In the present work, we have demonstrated that, by adding the pore partition agent, 2,4,6-tris(4-pyridyl)pyridine (TPY) during synthesis of the bimetallic Fe/Co-MIL-88(NH<sub>2</sub>) MOF to block the open metal sites, a highly porous MOF of Fe/Co-TPY-MIL-88(NH<sub>2</sub>) can be produced. This material also exhibits high stability in basic solutions and biofluids and possesses high peroxidase-mimicking activity, which can be utilized to produce long-lasting chemiluminescence (CL) from luminol and H<sub>2</sub>O<sub>2</sub>. Moreover, acting as the peroxidase-mimic, the Fe/Co-TPY-MIL-88(NH<sub>2</sub>) MOF can form the enzymatic cascade with glucose oxidase (GOx) for biomarker detection. When applied to detect extracellular vesicles (EVs), the MOF material and GOx are brought to the proximity on the EVs through two surface proteins, which triggers the enzyme cascade to produce high CL from glucose and luminol. EVs within the concentration range of  $5 \times 10^5$  -  $4 \times 10^7$  particles/mL can be detected, and the method can be used to analyze EV contents in human serum without sample preparation and EV purification. Overall, our work demonstrates that the high versatility and tunability of the MOF structures could bring in significant benefits to biosensing and enable ultrasensitive detection of biomarkers with judicious material designs.

Enzymatic cascade reactions involve two or more enzymes that function sequentially and transform reactants successively in one reactor. They offer high reaction efficiency, because of the enrichment of reactants localizing nearby the enzymes, complete mass transfer between different enzymatic reactions, and reduce intermediate decomposition.<sup>1-2</sup> Recently, extensive works have been focused on substituting the natural enzymes with the enzyme-mimicking nanomaterials, i.e. nanozymes,<sup>3</sup> in multi-enzyme reactions for their applications in detection of diverse biomarkers, including glucose, 5-7 acetylcholine, viral antigens, and tumor proteins, 10 because of their high activity, superior tunability, and low cost.<sup>3-4</sup> Among different designs of nanozymes, Metal-Organic Frameworks (MOFs) are one unique group of materials that deliver many advantages: they have abundant active catalytic sites per unit volume of the material, are capable of generating high signals through enzymatic reactions; and they can be formed by a variety of chemicals, including those with good biocompatibility as well as rich functional groups for biomolecule conjugation. 11-13 Furthermore, the high specific surface area, tunable pore size, and adjustable surface property of MOFs can assist with target separation and enrichment, as demonstrated in separation of biomolecules like DNA, <sup>14</sup> peptide, <sup>15</sup> and exosome, <sup>16</sup> from the complex sample matrix by MOFs with high stability in aqueous environments. With the dualfunctionality of target separation and signal production, MOFs are ideal choices to construct sensing platforms for diverse analytes.

In our previous work,<sup>17</sup> we developed the bimetallic MOF of Fe/Co-MIL-88(NH<sub>2</sub>) and demonstrated that the addition of Co(II) can greatly enhance the peroxidase-like activity of the MOF compared to the monometallic Fe-MIL-88(NH<sub>2</sub>), owing to the synergistic action of Co(II) and Fe(III) in the Fenton-like reactions. The peroxidase-mimicking MOF can be coupled with glucose oxidase (GOx) to form the cascade reaction system, and be applied for colorimetric

detection of a promising biomarker family, extracellular vesicles (EVs) $^{18}$  with a limit of detection (LOD)  $\sim 1 \times 10^5$  EV particles/mL. However, the dynamic range of detection using Fe/Co-MIL-88(NH<sub>2</sub>) is very narrow, spanning over only one order of magnitude. We suspect that, since the abundant unsaturated metal sites in the structure of MIL-88(NH<sub>2</sub>) MOF are susceptible to the attack from Lewis bases, this material may be unstable in aqueous solutions and complex matrices that contain rich chelators, and may not stand the burst production of  $H_2O_2$  in proximity when the analyte concentrations are high.

Pore space partition strategy that entails the insertion of a pore-partition agent in the framework has been applied to the MIL-88 (*acs* topology net) series MOF to produce the *pacs* (partitioned *acs*) MOFs with much improved stability and performance for gas separation. Herein, we introduce the pore partition agent, 2,4,6-tris(4-pyridyl)pyridine (TPY), to the bimetallic Fe/Co-MIL-88(NH<sub>2</sub>) MOF to form the Fe/Co-TPY-MIL-88(NH<sub>2</sub>) MOF. We prove that, this material possesses several advantages compared to the no-TPY counterpart: 1) it is much more porous and shows > 16 folds higher surface area per unit mass; 2) it exhibits much higher stability in basic solutions and in protein-rich matrices, like serum, while maintaining high peroxidase-like activity; 3) it can catalyze chemiluminescence (CL) production from luminol at pH 10 as a peroxidase-mimic, which cannot be done with the no-TPY MOF, and the resultant CL can last for tens of minutes; and 4) when applied to detect EVs, it increases the dynamic range by one order of magnitude.

## **Experimental Section**

**Materials.** Ferric(III) chloride, 6-hydrate (FeCl<sub>3</sub> · 6H<sub>2</sub>O, 98.1%) was acquired from J. T. Baker (Phillipsburg, NJ). Cobalt(II) nitrate hexahydrate (Co(NO<sub>3</sub>)<sub>2</sub> · 6H<sub>2</sub>O, 99%) was purchased

from Acros. Sodium chloride, potassium phosphate dibasic salt (anhydrous), acetic acid, N,N-Dimethylacetamide (DMA), and N,N-dimethylformamide (DMF) were purchased from Fisher Scientific (Waltham, MA). The following chemicals, 2-aminoterephthalic acid (H<sub>2</sub>(NH<sub>2</sub>)BDC), 3,3', 5,5"-tetramethylbenzidine (TMB), polyethylene glycol 400, potassium chloride, glycine (for electrophoresis, ≥99%) and glutaraldehyde, were from Sigma-Aldrich (Saint Louis, MI). Chemicals of 2,4,6-tris(4-pyridyl)pyridine (TPY), and 1,3-dimethyl-3,4,5,6-tetrahydro-2(1H)pyrimidinone (N,N-Dimethylpropyleneurea, DMPU) were purchased from TCI; and 1,1,1,5,5,5hexafluoro-2,4-pentanedione (HFP) were purchased from Alfa Aesar. Ethanol (EtOH, Anhydrous) was from KOPTEC. The amino group modified CD63 aptamer was produced by IDT, Inc. (Coralville, IA). The mouse anti-human CD9 (Clone MM2/57) and HRP were obtained from Sino Biological (Beijing, China) and Cell Signaling Technology (Danvers, MA), respectively. Streptavidin was purchased from Thermo Fisher Scientific (Waltham, MA). All chemicals were at the analytical reagent grade and used without further purification. Ultrapure water with electric resistance  $> 18.2 \text{ M}\Omega$  was produced by the Millipore Milli-Q water purification system (Billerica, MA).

Synthesis and activation of Fe/Co-TPY-MIL-88(NH<sub>2</sub>). The MOF materials were prepared via a solvothermal method. In a typical approach for the production of the bimetallic Fe/Co-TPY- MIL-88(NH<sub>2</sub>), 0.041 g FeCl<sub>3</sub> · 6H<sub>2</sub>O, 0.042 g Co(NO<sub>3</sub>)<sub>2</sub> · 6H<sub>2</sub>O, 0.030 g TPY and 0.056 g H<sub>2</sub>(NH<sub>2</sub>)BDC were dissolved in 4.007 g DMA and 2.001 g DMPU in a 23-mL glass bottle, then added 6 small drops HFP, stirred for ~40 min, and then heated in 140 °C for 24 hrs. After being cooled to room temperature, the brown-color crystals Fe/Co-TPY-MIL-88(NH<sub>2</sub>) were washed with DMF or DMA, collected by centrifugation, and dried at room temperature. MOF crystals were washed twice with ethanol at 60 °C or room temperature and then dried by vacuum to

remove the residual solvents that may impede the subsequent enzyme activity measurement and sensing performance. Fe/Co-MIL-88(NH<sub>2</sub>) was prepared as literature described (condition 1)<sup>17</sup> to be compared with the newly designed Fe/Co-TPY-MIL-88(NH<sub>2</sub>) for stability, activity, and sensing performance. Fe/Co-MIL-88(NH<sub>2</sub>) used for N<sub>2</sub> 77 K adsorption test was prepared by condition 2, which was slightly different from condition 1, see **Figure S4** caption text. Both samples synthesized by condition 1 and condition 2 have Fe/Co-MIL-88(NH<sub>2</sub>) structural topology as verified by Powder X-ray Diffraction.

Characterization of Fe/Co-TPY-MIL-88(NH<sub>2</sub>). The phase purity of Fe/Co-TPY-MIL-88(NH<sub>2</sub>) was examined by Powder X-ray Diffraction (PXRD). Most of the Powder X-ray diffraction experiments were performed on a Bruker D2 Phaser diffractometer, which was operating at 30 kV and 10 mA (Cu Kα radiation, λ = 1.5418 Å). The data collection was performed at room temperature in the range from 5° to 40° with a step size of ~0.020°. The PXRD experiments in Figure S3b were performed on a different instrument (see Figure S3 caption text). The simulated PXRD of Fe/Co-TPY-MIL-88(NH<sub>2</sub>) was obtained from the Fe-TPY-MIL-88(NH<sub>2</sub>) single crystal data.<sup>23</sup> Transmission Electron Microscopy (TEM) was done by the Thermo Scientific Talos L120C TEM equipment with Thermo Scientific CETA 16 4K×4K CMOS camera. Zeta-potential measurement and dynamic light scattering (DLS) were performed on a Zetasizer nano ZS90 (Malvern Instruments).

Brunauer–Emmett–Teller (BET) surface area was measured by the  $N_2$  77 K adsorption isotherm carried out on Micromeritics ASAP 2020 PLUS Physisorption Analyzer, and BET surface area was calculated from the desorption/adsorption curves by the BET equation (The points chosen to ensure that C always > 0, and correlation coefficient always > 0.999). For the Fe/Co-TPY-MIL-88(NH<sub>2</sub>) MOF, the material was immersed in ethanol for  $\sim$  3 days, with the

solution exchanged to a fresh preparation every day, and then degassed under vacuum at 60 °C for  $\sim 12.5$  hrs. For the Fe/Co-MIL-88(NH<sub>2</sub>) MOF, after the same ethanol treatment, it was dried by vacuum and then degassed under vacuum at 60 °C for  $\sim 14$  hrs.

MOF stability in different pH was evaluated by inductively coupled plasma optical emission spectrometry (ICP-OES). The MOF of 2.5 mg was suspended in 12.5 mL buffer for 15 min, and the supernatant was collected and mixed with 0.269 mL 70% nitric acid, 5 mL of which was used for ICP-OES analysis.

**Peroxidase-like activity evaluation and enzyme kinetics analysis of Fe/Co-TPY-MIL-88(NH<sub>2</sub>).** The peroxidase-like activity of the MOF materials was evaluated using the reaction between H<sub>2</sub>O<sub>2</sub> and 3,3′,5,5′-tetramethylbenzidine (TMB). In brief, 50 μg/mL MOF, 1 mM TMB, and H<sub>2</sub>O<sub>2</sub> at various concentrations (0, 0.005, 0.05, 0.1, 0.5 and 1 mM) were added to 0.4 mL of the NaAc-HAc buffer (200 mM, pH 4.1). The mixture was incubated at 37 °C for 15 min, and the visible light absorbance at 652 nm of the TMB oxidation product, i.e., oxTMB, was read in the BioTek Synergy HT microplate reader (Agilent).

The steady-state kinetics assays were performed as follows. The Fe/Co-TPY-MIL-88(NH<sub>2</sub>) going through the activation process was prepared at the concentration of 50 μg/mL in 100 μL of 200 mM NaAc-HAc buffer (pH 4.1). Then 1.0 mM TMB and H<sub>2</sub>O<sub>2</sub> at various concentrations (0, 0.05, 0.1, 0.5, 1.0, and 10 mM) were added and incubated at 37 °C. A time-course mode was used to monitor the absorbance change at 652 nm with a 10 s interval for 15 min in the BioTek Synergy HT microplate reader. The Beer-Lambert law was used to convert the absorbance to oxTMB concentration using the molar absorptivity at 652 nm of oxTMB (39,000 M<sup>-1</sup> · cm<sup>-1</sup>)<sup>24</sup> and the optical length of 0.233 cm of the 96 well plates. The concentration change at unit time within the first 15 min period was then calculated to represent the initial velocity (V).

Preparation of Fe/Co-TPY-MIL-88(NH<sub>2</sub>)/aptamer bioconjugate. Aptamer conjugation started by dispersing 35 mg Fe/Co-TPY-MIL-88(NH<sub>2</sub>) in 20 mL 1× PBS and adding 100 μL glutaraldehyde. After stirring the solution for 2 hrs, the solid was centrifuged, washed with 1× PBS 2 times, and dispersed in 2 mL 1× PBS. Next, 10 μL of 0.1 mM aptamer was added to the mixture, and the solution was put on a rotating plate and shaken overnight. The Fe/Co-TPY-MIL-88(NH<sub>2</sub>)/aptamer conjugate was then collected by centrifugation (20,000 g, 3 min) and redispersed in 2 mL 0.1 M glycine buffer containing 32 mM PEG(NH<sub>2</sub>) for 1 hr to passivate the MOF surface.

EV detection using Fe/Co-TPY-MIL-88(NH<sub>2</sub>) in enzyme cascades. Twenty μL of the EV sample was mixed with 170 μL of the Fe/Co-TPY- MIL-88(NH<sub>2</sub>)/aptamer bioconjugate at 17.5 mg/mL and 10 μL of the biotin-anti-CD9 antibody (or biotin-anti-HER2 antibody) solution at 0.10 mg/mL. The mixture was shaken at room temperature for 3 hrs. The MOFs with the bound EVs and proteins was centrifuged down (20,000 g, 3 min) and resuspended in 100 μL of the streptavidin solution at 0.017 mg/mL. After 1-hr incubation, the product was centrifuged down (20,000 g, 3 min), washed with 1× PBS once, and mixed with 100 μL of the biotinylated GOx at 0.013 mg/mL. After two washes with 1× PBS, the final product was resuspended in 1× PBS, 25 μL of which was mixed with 25 μL luminol (0.128 mM). Fifty μL glucose (2 mM) was injected into mixture before being tested in the Promega GloMax Multiplus Plate Reader. Luminescence was collected within the wavelength range of 350-650 nm.

## **Results and Discussions**

Design and characterization of the bimetallic Fe/Co-TPY-MIL-88(NH<sub>2</sub>). Many MOFs have been found to possess high peroxidase-mimicking activity and are capable of generating

high signals to enable sensing of low-abundant biomarkers, as what we reported previously for the Fe/Co-MIL-88(NH<sub>2</sub>) MOF.<sup>17</sup> However, one big hurdle in applying MOFs in biomedical fields, including in biosensing, is that they contain unsaturated, open metal sites, which could be easily attacked by electron-rich ligands such as water molecule, hydroxide anion and biomolecules in clinical samples, reducing the MOF stability in such environments. It has been reported that, with the insertion of a second ligand, more metal-ligand bonds could be formed to block the open metal sites and improve the stability of MOF.<sup>25-27</sup> The second ligand should match the size and symmetry of the geometrical pattern of the framework coordination sites and be compatible with the dimension of the channels formed by the first ligand to realize pore space partition. In Fe/Co-MIL-88(NH<sub>2</sub>), the unsaturated, open metal sites could form three metalligand bonds with three different ligand atoms on each layer along the ab plane. These metalligand bonds are in the manner of C3 symmetry and point to the center of the hexagonal channel. A planar tritopic ligand with C3 symmetry like TPY is ideal to fit such geometric features that to saturate the open metal sites, <sup>19</sup> and thus was chosen in the present work to enhance the stability of the bimetallic MOF (Figure S1) and improve its performance in biosensing.

The bimetallic Fe/Co-TPY-MIL-88(NH<sub>2</sub>) was then synthesized by the solvothermal method, as described in the Experimental Section. Fe(III) and Co(II) can coordinate with the carboxyl groups on the NH<sub>2</sub>BDC<sup>2-</sup> ligands, forming the trinuclear transition metal (TM) clusters (TM = Fe and Co). In addition, each TPY ligand coordinates with the three metal ions by its three pyridyl ends, giving a rigid framework (**Figure 1a**). The as-synthesized Fe/Co-TPY-MIL-88(NH<sub>2</sub>) MOF was initially distributed in the organic solvents used for synthesis. The stagnant organic solvent that stayed in the pore space of MOF was removed by soaking the MOF in ethanol and then drying it in vacuum. This process is termed activation, which did not alter the MOF size and

structure (**Figure S3**), and the "activated" materials were characterized and used throughout the present work.

Examination by TEM reveals that the Fe/Co-TPY-MIL-88(NH<sub>2</sub>) MOF exhibits a uniform, hexagon shape with the edge length about 500 nm (**Fig. 1b**); and DLS measurement in distilled water gives out an average hydrodynamic diameter of 1.8 µm (**Figure S3a and Table S1**). It is not expected that the hydration size measured by DLS for non-spherical particles would match exactly with that from TEM which has no solvent present.<sup>28</sup> Still, the much larger hydration size observed in DLS likely reflects some degrees of aggregation of the Fe/Co-TPY-MIL-88(NH<sub>2</sub>) MOF in the aqueous environment: the zeta-potential of the TPY MOF was lower than that of the no-TPY counterpart (**Table S1**).

PXRD was performed to characterize the crystal structure. The peaks of the Fe/Co-TPY-MIL-88(NH<sub>2</sub>) match well with those of the simulated Fe-TPY-MIL-88(NH<sub>2</sub>) spectrum, which confirms that the synthesized Fe/Co-TPY-MIL-88(NH<sub>2</sub>) shares the same topology with Fe-TPY-MIL-88(NH<sub>2</sub>) (Fig. 1c). In addition, the PXRD patterns of the MIL-88 MOF with or without TPY (Fig. 1c and Figure S4a) show distinct differences. For Fe/Co-TPY-MIL-88(NH<sub>2</sub>), four characteristic peaks at the low angles, (010), (011), (-120), and (002), are present, indicating the MOF belongs to the *pacs* class.<sup>19-22</sup> These peaks are different from the PXRD of the no-TPY MOF. Moreover, the BET surface area of Fe/Co-TPY-MIL-88(NH<sub>2</sub>) was found to be 1300 m<sup>2</sup>/g, ~ 16 times of that of the no-TPY MOF (Figure 1d). The high porosity of Fe/Co-TPY-MIL-88(NH<sub>2</sub>) agrees well with the results reported in literature for the *pacs* MOF materials.<sup>29</sup> Both the PXRD and BET data support that, TPY should have successfully participated in constructing the framework of Fe/Co-TPY-MIL-88(NH<sub>2</sub>).

Furthermore, we carried out the EDS line scan analysis (**Figure S2**) and confirmed the coexistence of Fe (0.70 keV) and Co (0.77 keV) in the Fe/Co-TPY- MIL-88(NH<sub>2</sub>) framework. The atomic% of Fe and Co was found to be 1.65 % and 1.36 %, respectively, while the mole ratio of the two metals added to the synthesis solution was 1:1. The weight% of Fe was around 6.55 %, with that of Co being about 5.69 %.

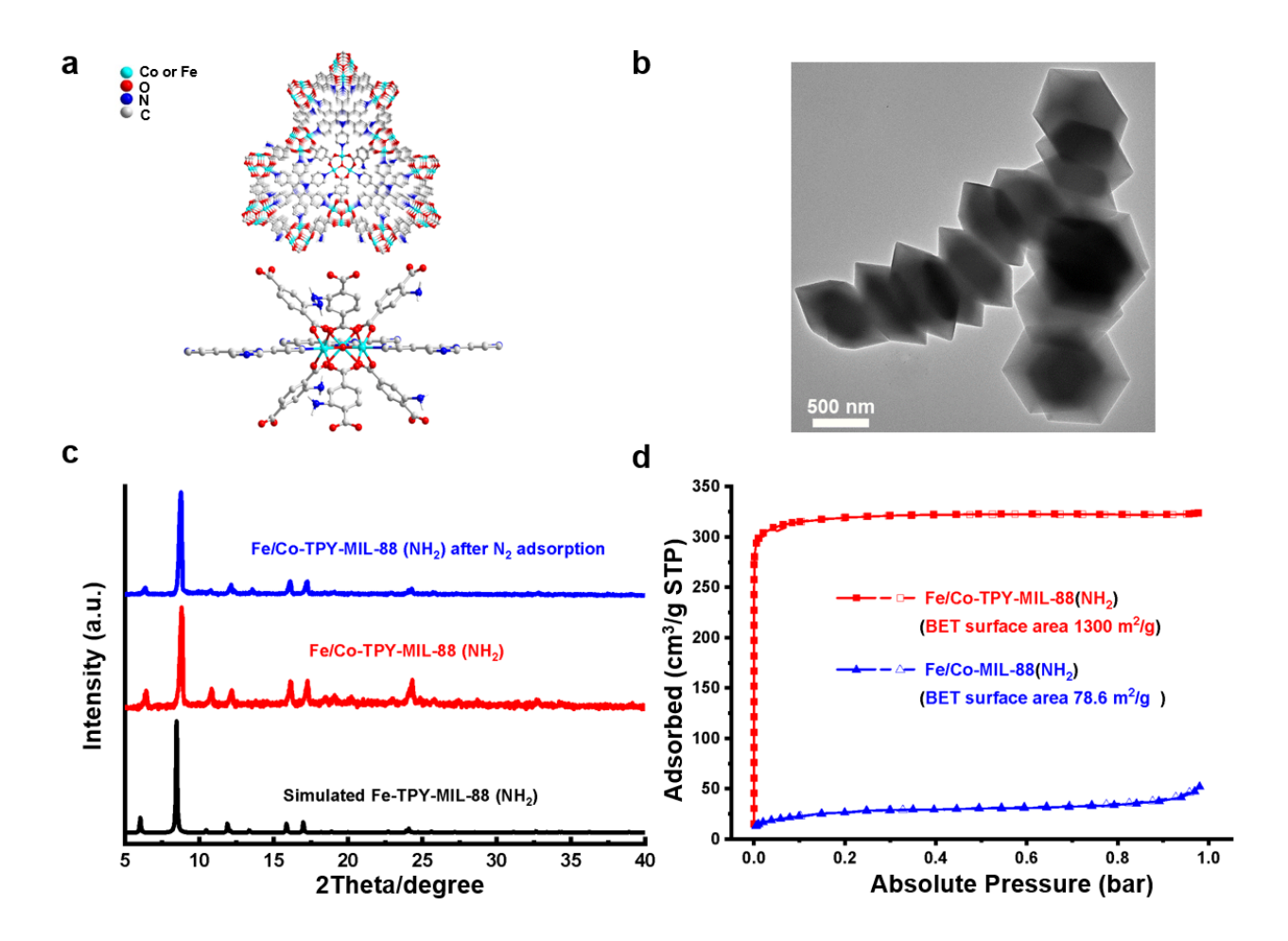


Figure 1. MOF characterization. a) Structure schematic diagram; b) TEM image of Fe/Co-TPY-MIL-88(NH<sub>2</sub>) (scale bar = 500 nm); c) PXRD measurement of Fe/Co-TPY-MIL-88(NH<sub>2</sub>) (before and after BET measurement, along with the simulated PXRD result of Fe-TPY-MIL-88(NH<sub>2</sub>); and d) N<sub>2</sub> adsorption isotherms at 77 K for Fe/Co-TPY-MIL-88(NH<sub>2</sub>) and Fe/Co- MIL-88(NH<sub>2</sub>). The simulated result was

reprinted from Wei, Y.-S.; Zhang, M.; Kitta, M.; Liu, Z.; Horike, S.; Xu, Q., J. Am. Chem. Soc. 2019, 141, 7906-7916 (Ref. 23). Copyright 2019 American Chemical Society.

Evaluation of the peroxidase-like activity of Fe/Co-TPY-MIL-88(NH<sub>2</sub>). To assess the impact on the peroxidase-like activity imposed by the addition of the second ligand TPY, we examined the model reaction of TMB oxidation into the blue oxTMB by H<sub>2</sub>O<sub>2</sub> catalyzed by Fe/Co-TPY-MIL-88(NH<sub>2</sub>) (Figure 2a). As seen from Figure S5, the visible light absorption at 652 nm for oxTMB changed from 0 to 0.075 with the addition of 50 μg/mL Fe/Co-TPY-MIL-88(NH<sub>2</sub>) to 1.0 mM TMB in 200 mM NaAc-HAc buffer at pH 4.1; and then to 0.41 with 1.0 mM H<sub>2</sub>O<sub>2</sub> added. These results well prove that the Fe/Co-TPY-MIL-88(NH<sub>2</sub>) could act like a peroxidase to catalyze TMB oxidation by H<sub>2</sub>O<sub>2</sub>. The low signal produced without H<sub>2</sub>O<sub>2</sub> is the result of oxidase-mimicking activity.<sup>30</sup> Steady-state kinetic analysis was also carried out. The absorbance change at 652 nm was monitored with the MOF and one of the reactants (TMB or H<sub>2</sub>O<sub>2</sub>) added at fixed concentrations to react with varying concentrations of the other reactant. The initial production rate (V in µM.min<sup>-1</sup>) of oxTMB within the first 15-min reaction window was plotted against the H<sub>2</sub>O<sub>2</sub> concentrations ([S]) to yield the Michaelis-Menten curve (Figure 2b). Rearranging Figure 2b to the linear Lineweaver-Burk plot (Figure S6) can attain the Michaelis constant (K<sub>m</sub>) and maximum reaction velocity (V<sub>max</sub>) from its slope and Y-intercept:  $[1/V = (K_m/V_{max}) \times (1/[S]) + 1/V_{max}]$ . The molarity of the MOF was estimated by counting the number of MOF particles under an optical microscope, which was then divided by V<sub>max</sub> (Figure 2c) to calculate the catalytic constant ( $k_{cat}$ ) of the bimetallic Fe/Co-TPY-MIL-88(NH<sub>2</sub>). The K<sub>m</sub> and  $k_{\text{cat}}$  against TMB, was also measured (Figure S7). We compared the  $K_{\text{m}}$  and  $k_{\text{cat}}$  values with those of Fe/Co-MIL-88(NH<sub>2</sub>) acquired in our previous work.<sup>17</sup> As shown in Figure 2c, a K<sub>m</sub> of 0.697 mM to H<sub>2</sub>O<sub>2</sub> was found for Fe/Co-TPY-MIL-88(NH<sub>2</sub>), close to that of Fe/Co-MIL- $88(NH_2)$ ; but the  $K_m$  of Fe/Co-TPY-MIL- $88(NH_2)$  to TMB was about 4 times larger. This

comparison indicates that blocking the open metal sites by ligand did not affect the affinity of  $H_2O_2$  to MOF, but reduced the affinity of TMB. This is probably due to the difference in TMB interaction with TPY and the original ligand of 2- aminoterephthalic acid, which has two carboxyl groups to interact with the primary amines on TMB.

Surprisingly, the k<sub>cat</sub> of Fe/Co-TPY-MIL-88(NH<sub>2</sub>) measured with varying H<sub>2</sub>O<sub>2</sub> or TMB concentrations were 150-200 times larger than those of Fe/Co-MIL-88(NH<sub>2</sub>). One cause for the higher enzymatic activity could be its relatively higher amount of the more active metal of Co compared to Fe/Co-MIL-88(NH<sub>2</sub>): the EDS results illustrate that the Fe: Co atom ratio in Fe/Co-TPY-MIL-88(NH<sub>2</sub>) was close to 1:1, while it was 3:1 in Fe/Co-MIL-88(NH<sub>2</sub>). Additionally, by introducing TPY in Fe/Co-MIL-88 (NH<sub>2</sub>), TPY occupies the open metal site on metal trimers and also because of TPY, the Fe/Co-TPY-MIL-88(NH<sub>2</sub>) MOF shows much enhanced stability, rigidity and porosity. Without TPY, Fe/Co-MIL-88 (NH<sub>2</sub>) is quite flexible with limited pore access. 31-33 As a result, the BET surface area of Fe/Co-TPY-MIL-88(NH<sub>2</sub>) is 1,300 m<sup>2</sup>/g, which is much larger than that of Fe/Co- MIL-88(NH<sub>2</sub>) MOF. The pore width has a peak value of 0.59 nm (Fig. S4b). With higher surface area and accessible porous structure in Fe/Co-TPY-MIL-88(NH<sub>2</sub>) MOF, the active metal sites are more accessible to the substrates and help enhance the peroxidase-mimicking activity. The pore size distribution profile of the Fe/Co-TPY-MIL-88(NH<sub>2</sub>) MOF calculated with the Density Functional Theory (DFT) using the N<sub>2</sub> adsorption data is shown in Fig. S4b. The Fe/Co-TPY-MIL-88(NH<sub>2</sub>) MOF has the pore width distribution at around 5.9 Å (Fig. S4b), and has a much larger BET surface area. With the more porous structure, the active metal site in the TPY MOF should be more accessible to the substrates (the topological polar surface area of TMB and H<sub>2</sub>O<sub>2</sub> is 52 and 40.5 Å<sup>2</sup>, respectively (https://pubchem.ncbi.nlm.nih.gov)), enhancing the peroxidase-mimicking activity. On the other

hand,  $k_{cat}$  indicates the product turn-over rate generated per mole of the "enzyme" per second. Since the hydration size of the TPY MOF enlarged by ~ 2.5 folds (1.8 ± 0.05  $\mu$ m of the TPY MOF vs. 0.70 ± 0.1  $\mu$ m of the no-TPY MOF, **Table S1**) compared to the no-TPY MOF, each mole of the TPY MOF would have more metals to result in the much larger  $k_{cat}$  value.

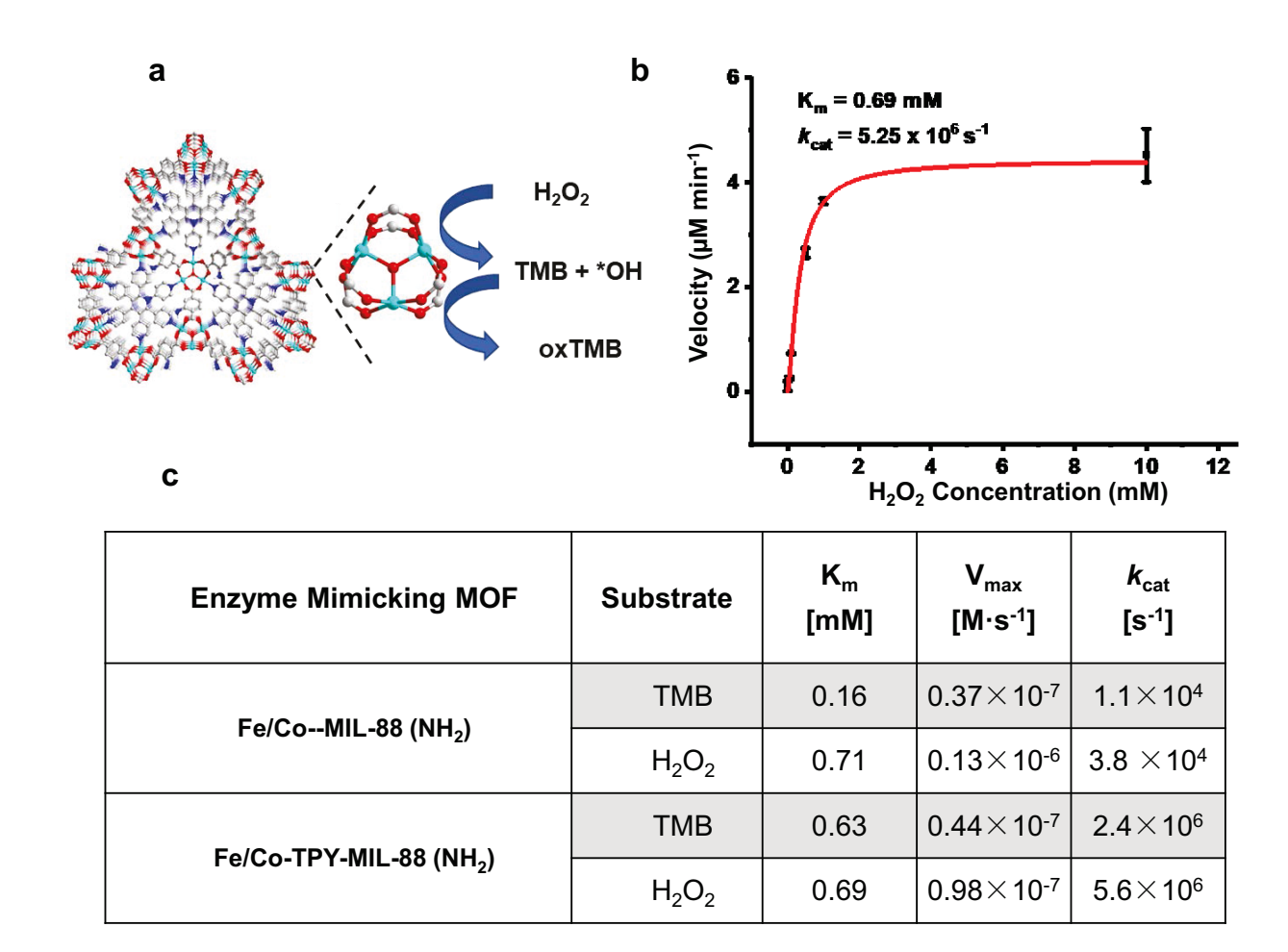


Figure 2. Peroxidase-like activity of Fe/Co-TPY-MIL-88(NH<sub>2</sub>). a) Schematic illustration of the reaction between TMB and  $H_2O_2$  catalyzed by MOF; b) Plotting the initial reaction velocity calculated from the absorbance change against the corresponding  $H_2O_2$  concentrations. 1.0 mM TMB, 50 µg/mL Fe/Co-TPY-MIL-88(NH<sub>2</sub>), and 0.005 – 10 mM  $H_2O_2$ . All reactions were in 200 mM NaAc-HAc buffer at pH 4.1; c) Comparison of the catalytic parameters of Fe/Co-MIL-88 (NH<sub>2</sub>) and Fe/Co-TPY-MIL-88 (NH<sub>2</sub>).

Bimetallic Fe/Co-TPY- MIL-88 (NH<sub>2</sub>) for CL generation by enzyme cascades. TMB is widely used as the substrate for peroxidase-based signaling in biosensing. While colorimetric detection has the advantages of high simplicity and low requirement for instrumentation, chemiluminescence produced by substrates like luminol is another attractive signaling strategy because of its high signal-to-background ratio. The mechanism of CL production from luminol catalyzed by transition metals through Fenton-like reactions has been widely studied. 34-36 Transition metals like  $Co^{2+}$  and  $Fe^{3+}$  can react with  $H_2O_2$  to produce radicals like  $OH \cdot .^{34-35}$ Luminol can undergo oxidation reaction with these reactive oxygen species to form the peroxyketal intermediate (LHOOH). 34-35 At a high pH value LHOOH is present in the anionic form that rapidly decomposes to generate the excited-state aminophatalate dianion (AP<sup>2-\*</sup>) which emits photons in the visible light range.<sup>36</sup> These proposed reaction pathways and previous experimental measurements all highlight the importance of an alkaline pH for high CL generation by luminol.<sup>34-36</sup> However, the highly basic condition could be detrimental to MOFs with open metal sites like the Fe/Co-MIL-88(NH<sub>2</sub>). We hypothesize that, with the open metal sites filled by TPY, the Fe/Co-TPY-MIL-88(NH<sub>2</sub>) MOF should gain sufficient stability and suitable for catalysis of CL production under basic pH. Indeed, after 15-min incubation (a time span equivalent to that in the cascade reaction) in the buffers having pH 7 and 10, only  $\sim 5\%$  and 10% of the total Co and Fe in the Fe/Co-TPY-MIL-88(NH<sub>2</sub>) MOF were released to the supernatant, respectively, tested by ICP-OES (Table S2). These percentages increased to 12% for Co and 29% for Fe when incubated at pH 12. Such tests were also attempted on the Fe/Co-MIL-88(NH<sub>2</sub>) MOF that contained no TPY, and rapid precipitation of the metal ions in their insoluble hydroxide forms was clearly observed. This further proves that, while Fe/Co- MIL-

88(NH<sub>2</sub>) MOF can remain stable at pH 4.1 and oxidize TMB for signal amplification in our previous work, it cannot be used for CL production.

We then assessed the capability of the Fe/Co-TPY-MIL-88(NH<sub>2</sub>) to catalyze CL generation from luminol in pH ranging from 5 to 12. We mixed 50 µg/mL Fe/Co-TPY-MIL-88(NH<sub>2</sub>) with 1.0 mM H<sub>2</sub>O<sub>2</sub> and 0.002 mM luminol in the buffers. We found that the signal-to-background ratio (CL/CL<sub>0</sub>) was very low at pH  $\leq$  8, and rapidly increased with pH  $\geq$  8, reaching a peak value at pH 10. This phenomenon agrees with those reported in the previous works and mechanism study. 34, 36 But, the CL dropped substantially at pH 11 and 12 (Figure 3b), which could be due to the significant damage to the MOF structure under the highly basic conditions. At pH 10, the MOF produced a CL signal  $\sim 10^4$  folds higher than that in the mixture of luminol/ $H_2O_2$  or luminol/Fe/Co-TPY-MIL-88(NH<sub>2</sub>) systems (Figure S8a). More interestingly, we found that CL production at this pH could last for at least 1 min (Fig. 3c). In contrast, the no-TPY MOF, Fe/Co-MIL-88(NH<sub>2</sub>), only produced a burst of CL that decades rapidly within 20 sec. The high stability of the TPY MOF, as well as the limited diffusion of the catalytic center and confined reactants within the porous MOF structures<sup>37-38</sup> could both contribute to the strong and long-lasting luminescence emission, which is favorable for accurate and sensitive CL analysis.<sup>39-40</sup> The optimal luminol concentration in the CL generation reaction was determined to be 0.032 mM (Fig. S8b).

We also tested whether the TPY MOF can be coupled with GOx to form an enzyme cascade for CL production (**Fig. 3a**). Since the optimal CL signaling pH is 10, to realize the one-pot reaction, GOx should still be active in this pH. Thus, we evaluated the GOx activity at various pHs by benzoquinone, which can replace  $O_2$  as an electron acceptor in the oxidation of  $\beta$ -d-glucose, and be converted to hydroquinone (HQ) to exhibit an absorbance peak at 289 nm (molar

absorptivity ( $\varepsilon_{HQ}$ ) = 2600 L·mol<sup>-1</sup>·cm<sup>-1</sup>).<sup>41-42</sup> The absorbance at 289 nm was monitored for one minute after mixing 0.00375 mg/mL GOx with 0.025% (w/v) benzoquinone and 0.5 M glucose; and the initial reaction velocity was calculated using the Beer-Lamber law and the  $\varepsilon_{HQ}$  value reported. Agreeing with the common reaction conditions found in literature, pH 5 gave the highest reaction rate, which decreased with increasing pH (**Fig. 3b**). More significant reaction rate drop was observed with pH beyond 11 and 12; and at pH 10, the reaction rate remains to be about 86% of the optimal value, supporting the feasibility of coupling both GOx and the MOF for CL production at pH 10.

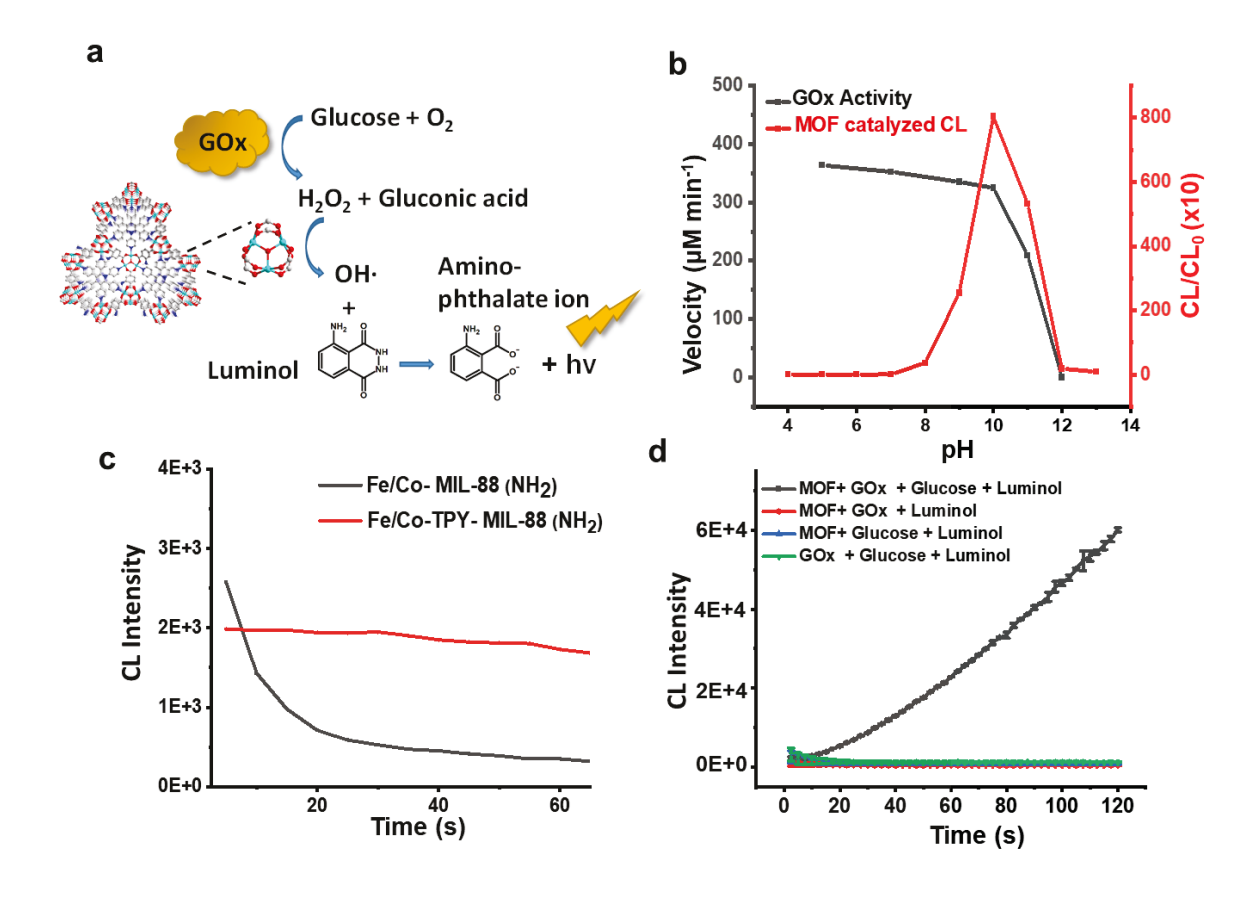


**Figure 3.** a) Schematic illustration of coupling Fe/Co-TPY-MIL-88 (NH<sub>2</sub>) and GOx to construct the enzymatic cascade reaction for CL signal generation; b) Effects of pH on the reaction velocity of the  $GO_x$  (black curve) and on the peroxidase-mimicking activity of MOF (red). CL collected at t = 60 sec, and

generated from the mixture of 0.002 mM luminol, 1 mM  $H_2O_2$ , and 50  $\mu$ g/mL MOF;  $CL_0$  was the signal measured without  $H_2O_2$ . GOx activity assessment reaction: 0.025% Benzoquinone, 0.5 M Glucose, 3.75  $\mu$ g/mL GOx, reaction time = 1 min. The buffers delivered different pH values: 10 mM acetate buffer (pH 4.0 & 5.0), 10 mM phosphate buffer (pH 6.0, 7.0, & 8.0), 10 mM borate buffer (pH 9.0 & 10.0), NaOH solution (pH 11.0, 12.0, & 13.0). c) Chemiluminescence generation using 50  $\mu$ g/ml Fe/Co-TPY-MIL-88 (NH<sub>2</sub>) or Fe/Co-MIL-88 (NH<sub>2</sub>), with 0.002 mM luminol and 1 mM  $H_2O_2$  in NaOH solution (pH 10.0); d) CL production observed with various combinations of , 1 mM glucose, 25  $\mu$ g /mL MOF, 2.5  $\mu$ g/mL GOx and 0.032 mM luminol in borate buffer (pH 10.0, 10 mM).

At last, we tested the enzymatic cascade reaction by mixing 25  $\mu$ g/mL Fe/Co-TPY-MIL-88(NH<sub>2</sub>) with 2.5  $\mu$ g/mL GOx, 1.0 mM glucose, and 0.032 mM luminol in 10 mM borate buffer at pH 10. CL production was monitored for 2 minutes. The CL signal rapidly increased with time, but negligible CL was observed without MOF, without glucose or without GOx (Fig. 3d). Similar to the long-lasting CL seen in Fig. 3c, at pH 10, the enzyme cascade also produced CL that reached a maximum emission at ~ 60 sec and maintained at ~ 50% of the maximum intensity for at least 30 min (Figure S9) with 25  $\mu$ g/mL MOF and 250  $\mu$ g/mL GOx in the reaction system. Agreeing with the pH test results shown in Fig. 3b, low CL was found from the enzyme cascade at other alkaline pH values. To further confirm the feasibility of using the enzymatic cascade reaction for biosensing, we spiked different amounts of GOx into the mixture of 25  $\mu$ g/mL MOF, 1 mM glucose, and 0.032 mM luminol in 10 mM borate buffer at pH 10, and collected the CL signal at 1 minute after mixing. The lowest GOx concentration detectible by the system was 0.15 nM (Figure S10).

**Detection of EVs in biological samples**. The high stability and excellent peroxidase-like activity of Fe/Co-TPY- MIL-88(NH<sub>2</sub>) should make it highly useful in biosensing. To prove this, we employed the MOF-based enzymatic cascade reaction for detection of EVs. EVs are

considered as promising circulating tumor markers owing to their critical roles in cancer progressing and metastasis, the inherent stability of EVs in circulation, and the diversity of EV cargos. 18, 43-44 We modified the Fe/Co-TPY-MIL-88(NH<sub>2</sub>) with the anti-CD63 aptamer for the capture of exosomes, an EV sub-family considered to be valuable in cancer diagnosis and quenched the residual reactive groups after glutaraldehyde activation by the NH<sub>2</sub>-modified polyethylene glycol (PEG-NH<sub>2</sub>) and glycine. The modification caused ~ 30% decrease in the CL signal produced by the enzyme cascade, but still the plateau CL was > 30 times higher than that obtained at t = 0 sec (Figure S11). We then optimized the conjugation conditions as well as the amount of the aptamer-conjugated MOF used for exosome binding (Figure S12). When applied to capture exosomes; the biotinylated anti-CD9 recognized another marker on exosome, CD9, which then bound to the streptavidin and biotinylated GOx to form the enzyme cascade for CL production (Figure 4a). Since the MOF can be quickly spun down using a common table-top centrifuge, it can be used to enrich the target into a small volume from a diluted sample before GOx binding: 99.92% of the exosome particles spiked in 200 µL 1× PBS was captured by the MOF after 3 hours incubation. This isolation efficiency was comparable to that from the commercial, 1-µm magnetic beads modified by the same aptamer (Fig. 4b).

We confirmed that the enzyme cascade can detect EVs dispersed in  $1 \times PBS$  at concentrations ranging from  $5 \times 10^5$  -  $4 \times 10^7$  particles/mL (**Fig. 4c**), using two surface markers, i.e. CD9 and HER2, for signaling, and capturing the EV subfamily, exosomes, using CD63. Such a detection range was about one order of magnitude wider than that  $(10^5 - 10^6 \text{ particles/mL})$  obtained with the Fe/Co-MIL-88(NH<sub>2</sub>) MOF,<sup>17</sup> and the slope of the linear curve plotted between signal change ratio and Log (EV concentration) was about 2.3 times larger, indicating faster signal change with target input (**Figure S13**). LOD calculated with the  $3\sigma$  method is  $1.26 \times 10^5$  particles/mL and

 $1.15 \times 10^5$  particles/mL for using CD9 and HER2 as the detection marker, respectively (**Fig. 4c**). These LODs are  $\sim 100$  times lower than the standard methods like ELISA and NTA for EV quantification. From Fig. 4c, we can also see the overall signal from detecting HER2 is lower than from CD9, indicating the lower abundance of HER2 than CD9 on the EVs. This is reasonable because HER2 is a tumor protein, which may not be present in all exosomes, while CD9 is another exosomal marker just like CD63. However, we anticipate using the specific tumor protein would identify those exosomes derived from tumor cells, and could be more specific in cancer diagnosis.

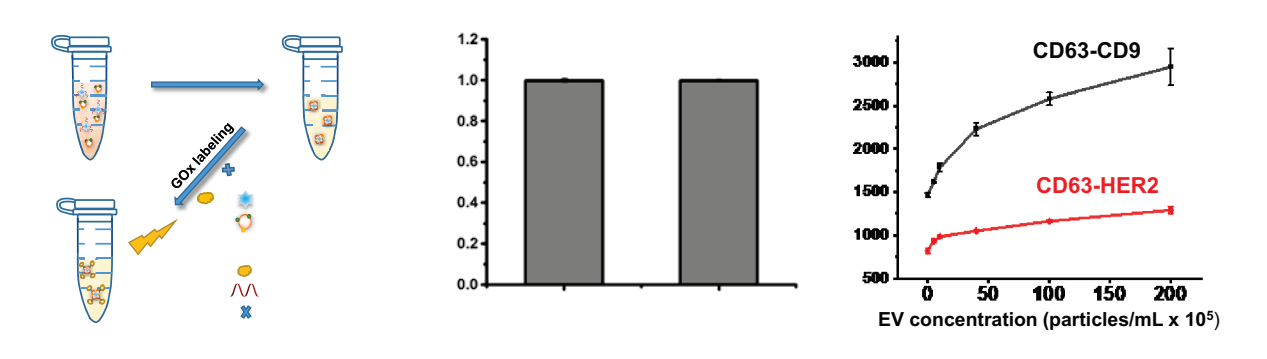
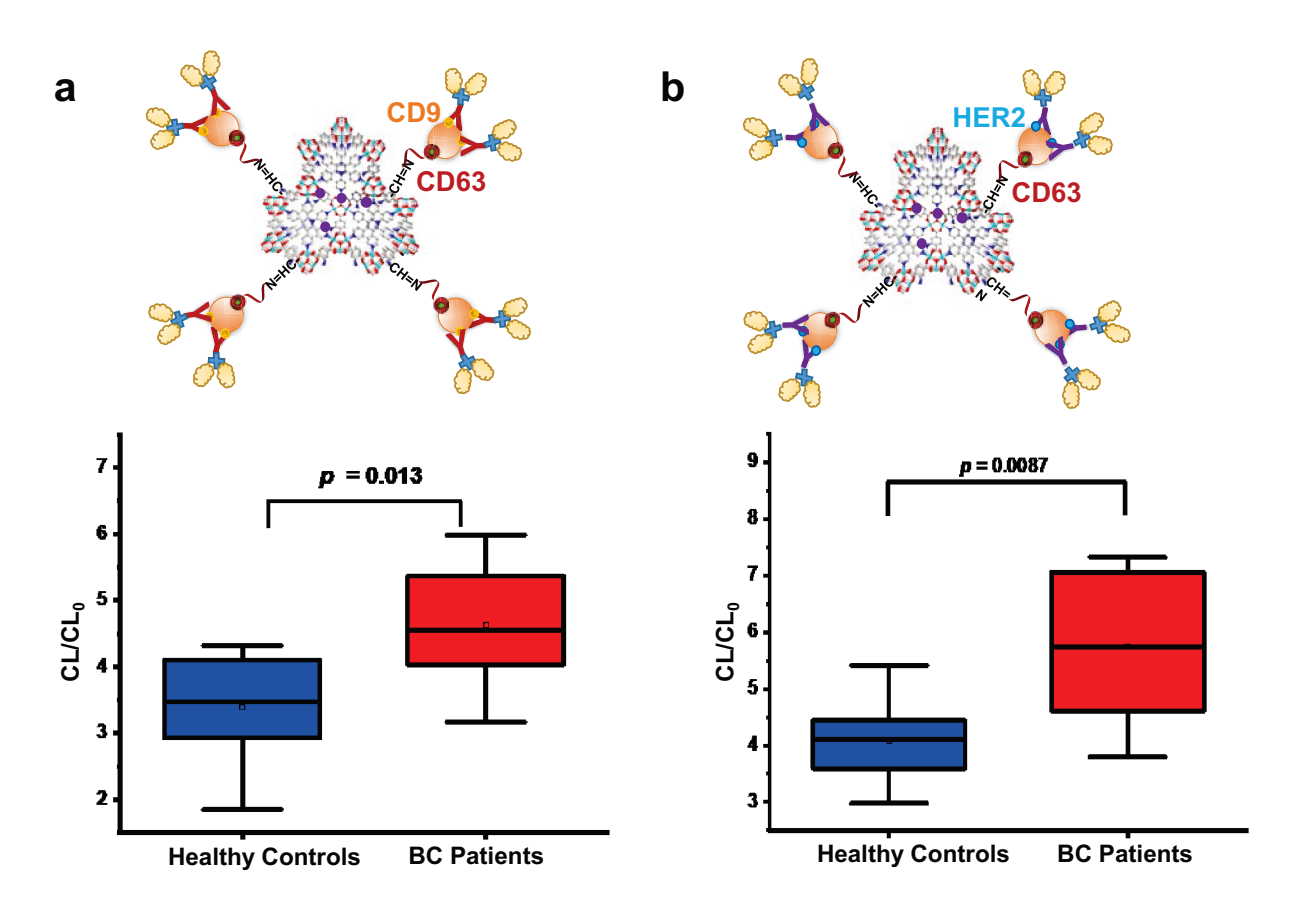


Figure 4. a) Scheme of EV detection facilitated by the cascade reaction between the peroxidase-mimicking Fe/Co-TPY-MIL-88(NH<sub>2</sub>) and GOx, b) EV recovery comparison for using MOF and magnetic beads (ave. diameter ~ 1 μm) for EV enrichment. Recovery was measured by quantifying the exosome concentration remained in the supernatant after 3-hr incubation of 1.6 × 10<sup>8</sup> EV particles with 2.975 mg MOF or beads in 200 mL 1× PBS using the TPY MOF-based assay. c) Calibration curves for detection of EVs dispersed in 1× PBS. EVs were captured by 3.0 mg anti-CD63 aptamer-conjugated MOF and bound to the biotinylated anti-CD9 (black curve) or anti-HER2 antibody (red curve), which was then recognized by the streptavidin-labeled GOx. Detection solution:1 mM glucose, 0.032 mM luminol, in 10 mM borate buffer (pH 10.0).

We then applied the assay to detect exosomes in human sera collected from breast cancer patients and healthy people (n = 8 for each cohort). The exosomes carrying both CD63 and CD9,

or both CD63 and HER2, were tested. We found that the exosome concentrations in these clinical samples were much higher than the upper detection limit of our assay, and far less than 1  $\mu$ L serum was needed for each measurement. The samples collected from BC patients contained significantly higher exosome concentrations than those from the healthy controls (**Figure 5a**). The CD63-HER2 combination showed a slightly lower p value (p = 0.0087, Student's t test) than that obtained with the CD63-CD9-based assay (p = 0.013). These results support that Fe/Co-TPY-MIL-88(NH<sub>2</sub>) can enable sensitive biomarker detection in complex biological matrices with ultra-low sample consumption and should possess high potential in clinical applications.



**Figure 5.** Application of Fe/Co-TPY-MIL-88(NH<sub>2</sub>) for EV detection in the sera samples from healthy controls (n=8) and breast cancer patients (n=8), targeting the marker combination of a) CD63-CD9 and b) CD63-HER2, respectively. Detection solution:1 mM glucose, 0.032 mM luminol, in 10 mM borate buffer (pH 10.0). CL and CL<sub>0</sub> were the signals measured at t = 60 sec and t = 10 sec, respectively.

## Conclusion

In the present work, the Fe/Co-TPY-MIL-88(NH<sub>2</sub>) MOF was constructed using the pore partition agent TPY to saturate the open metal site and enhance the stability of the MOF structure in bioassays. Addition of TPY does not affect the peroxidase-mimicking activity of the MOF, and the resultant high stability in basic solutions permits it to work with GOx in the cascade enzymatic reactions to generate CL at a basic pH of 10 by inputting glucose. When applied to detect a group of biomarkers, exosomes, a dynamic range one order of magnitude wider than that obtained with Fe/Co-MIL-88(NH<sub>2</sub>) was obtained with a comparable LOD. These results support that, the high versatility and tunability of the MOF structures could bring in significant benefits to biosensing and enable ultrasensitive detection of biomarkers with judicious material designs. Future improvements in assay performance can consider reducing the hydration size of the MOF by enhancing its hydrophilicity and amplifying the number of GOx bound to the MOF mediated by the target. In addition, superior to typical CL systems, both the stand-alone peroxidasemimicking activity of the Fe/Co-TPY-MIL-88(NH<sub>2</sub>) MOF and the cascade reaction system composed of the MOF and GOx can generate long-lasting CL. This property is worthy of further investigation for better understanding of the reaction mechanism and may benefit applications of such materials in areas other than biosensing, like light or energy production and biosynthesis.

## ASSOCIATED CONTENT

## **Supporting Information**

Additional data of material characterization, catalytic activity evaluation, CL generation by enzyme cascades; detection of GOx based on CL; assay optimization; and ion release from MOF

assessed by ICP-AES. This material is available free of charge via the Internet at <a href="http://pubs.acs.org">http://pubs.acs.org</a>.

### **Author Information**

## **Corresponding Author**

\* E-mail: pingyun.feng@ucr.edu; wenwan.zhong@ucr.edu

## Acknowledgements

The research work was supported by the National Science Foundation grant #CHE-1707347, UCR's Extramural Funding Opportunity Preparation Award (EFOPA), and City of Hope – UC Riverside Biomedical Research Initiative (CUBRI) to W. Zhong. We also acknowledge the support of the MOF synthesis and characterization by the US Department of Energy, Office of Basic Energy Sciences, Materials Sciences and Engineering Division under Award No. DE-SC0010596 (P.F.).

## Reference

- 1. Kucherenko, I. S.; Soldatkin, O. O.; Dzyadevych, S. V.; Soldatkin, A. P., Electrochemical Biosensors Based on Multienzyme Systems: Main Groups, Advantages and Limitations—a Review. *Anal. Chim. Acta* **2020**, *1111*, 114-131.
- 2. Vázquez-González, M.; Wang, C.; Willner, I., Biocatalytic Cascades Operating On Macromolecular Scaffolds and In Confined Environments. *Nat. Catalysis* **2020**, *3* (3), 256-273.
- 3. Zhang, X.; Li, G.; Chen, G.; Wu, D.; Wu, Y.; James, T. D., Enzyme Mimics for Engineered Biomimetic Cascade Nanoreactors: Mechanism, Applications, and Prospects. *Adv. Functional Mat.* **2021**, *31* (50), 2106139.
- 4. Cai, X.; Jiao, L.; Yan, H.; Wu, Y.; Gu, W.; Du, D.; Lin, Y.; Zhu, C., Nanozyme-Involved Biomimetic Cascade Catalysis for Biomedical Applications. *Mat. Today* **2021**, *44*, 211-228.
- 5. Liu, Y.; Zheng, Y.; Chen, Z.; Qin, Y.; Guo, R., High-Performance Integrated Enzyme Cascade Bioplatform Based on Protein–BiPt Nanochain@ Graphene Oxide Hybrid Guided One-Pot Self-Assembly Strtegy. *Small* **2019**, *15* (12), 1804987.
- 6. Sengupta, P.; Pramanik, K.; Datta, P.; Sarkar, P., Chemically Modified Carbon Nitride-Chitin-Acetic Acid Hybrid as a Metal-Free Bifunctional Nanozyme Cascade of Glucose Oxidase-Peroxidase for "Click Off" Colorimetric Detection of Peroxide and Glucose. *Biosens. Bioelectron.* **2020**, *154*, 112072.

- 7. Jiao, L.; Xu, W.; Yan, H.; Wu, Y.; Gu, W.; Li, H.; Du, D.; Lin, Y.; Zhu, C., A Dopamine-Induced Au Hydrogel Nanozyme for Enhanced Biomimetic Catalysis. *Chem. Comm.* **2019**, *55* (66), 9865-9868.
- 8. Wu, Y.; Wu, J.; Jiao, L.; Xu, W.; Wang, H.; Wei, X.; Gu, W.; Ren, G.; Zhang, N.; Zhang, Q., Cascade Reaction System Integrating Single-Atom Nanozymes with Abundant Cu Sites for Enhanced Biosensing. *Anal. Chem.* **2020**, *92* (4), 3373-3379.
- 9. Du, M.; Li, N.; Mao, G.; Liu, Y.; Wang, X.; Tian, S.; Hu, Q.; Ji, X.; Liu, Y.; He, Z., Self-Assembled Fluorescent Ce (III) Coordination Polymer as Ratiometric Probe for HIV Antigen Detection. *Anal. Chim. Acta* **2019**, *1084*, 116-122.
- 10. Xianyu, Y.; Chen, Y.; Jiang, X., Horseradish Peroxidase-Mediated, Iodide-Catalyzed Cascade Reaction for Plasmonic Immunoassays. *Anal. Chem.* **2015**, *87* (21), 10688-10692.
- 11. Xu, W.; Jiao, L.; Wu, Y.; Hu, L.; Gu, W.; Zhu, C., Metal-Organic Frameworks Enhance Biomimetic Cascade Catalysis for Biosensing. *Adv. Mat.* **2021**, *33* (22), 2005172.
- 12. Liang, J.; Liang, K., Multi-Enzyme Cascade Reactions in Metal-Organic Frameworks. *The Chemical Record* **2020**, *20* (10), 1100-1116.
- 13. Feng, Y.; Xu, Y.; Liu, S.; Wu, D.; Su, Z.; Chen, G.; Liu, J.; Li, G., Recent Advances in Enzyme Immobilization based on Novel Porous Framework Materials and Its Applications in Biosensing. *Coordination Chem. Rev.* **2022**, *459*, 214414.
- 14. Peng, S.; Bie, B.; Jia, H.; Tang, H.; Zhang, X.; Sun, Y.; Wei, Q.; Wu, F.; Yuan, Y.; Deng, H., Efficient Separation of Nucleic Acids with Different Secondary Structures by Metal–Organic Frameworks. *J. Am. Chem. Soc.* **2020**, *142* (11), 5049-5059.
- 15. Yang, S.-S.; Chang, Y.-J.; Zhang, H.; Yu, X.; Shang, W.; Chen, G.-Q.; Chen, D. D. Y.; Gu, Z.-Y., Enrichment of Phosphorylated Peptides with Metal—Organic Framework Nanosheets for Serum Profiling of Diabetes and Phosphoproteomics Analysis. *Anal. Chem.* **2018**, *90* (22), 13796-13805.
- 16. Zhang, L.; Wang, H.; Zhao, G.; Li, N.; Wang, X.; Li, Y.; Jia, Y.; Qiao, X., Anti-Tim4 Grafting Strongly Hydrophilic Metal—Organic Frameworks Immunoaffinity Flake for High-Efficiency Capture and Separation of Exosomes. *Anal. Chem.* **2021**, *93* (16), 6534-6543.
- 17. Jiang, Q.; Xiao, Y.; Hong, A. N.; Gao, Z.; Shen, Y.; Fan, Q.; Feng, P.; Zhong, W., Bimetallic Metal–Organic Framework Fe/Co-MIL-88 (NH2) Exhibiting High Peroxidase-like Activity and Its Application in Detection of Extracellular Vesicles. *ACS Appl. Mat. Interfaces* **2022**, *14* (37), 41800-41808.
- 18. Kalluri, R.; LeBleu, V. S., The Biology, Function, and Biomedical Applications of Exosomes. *Science* **2020**, *367* (6478), eaau6977.
- 19. Zhao, X.; Bu, X.; Zhai, Q.-G.; Tran, H.; Feng, P., Pore Space Partition by Symmetry-Matching Regulated Ligand Insertion and Dramatic Tuning on Carbon Dioxide Uptake. *J. Am. Chem. Soc.* **2015**, *137* (4), 1396-1399.
- 20. Yang, H.; Wang, Y.; Krishna, R.; Jia, X.; Wang, Y.; Hong, A. N.; Dang, C.; Castillo, H. E.; Bu, X.; Feng, P., Pore-Space-Partition-Enabled Exceptional Ethane Uptake and Ethane-Selective Ethane–Ethylene Separation. *J. Am. Chem. Soc.* **2020**, *142* (5), 2222-2227.
- 21. Yang, H.; Peng, F.; Hong, A. N.; Wang, Y.; Bu, X.; Feng, P., Ultrastable High-Connected Chromium Metal-Organic Frameworks. *J. Am. Chem. Soc.* **2021**, *143* (36), 14470-14474.
- 22. Xiao, Y.; Hong, A. N.; Chen, Y.; Yang, H.; Wang, Y.; Bu, X.; Feng, P., Developing Water-Stable Pore-Partitioned Metal-Organic Frameworks with Multi-Level Symmetry for High-Performance Sorption Applications. *Small* 2022, 2205119. https://doi.org/10.1002/smll.202205119.
- 23. Wei, Y.-S.; Zhang, M.; Kitta, M.; Liu, Z.; Horike, S.; Xu, Q., A Single-Crystal Open-Capsule Metal—Organic Framework. *J. Am. Chem. Soc.* **2019**, *141* (19), 7906-7916.
- 24. Jiang, B.; Duan, D.; Gao, L.; Zhou, M.; Fan, K.; Tang, Y.; Xi, J.; Bi, Y.; Tong, Z.; Gao, G. F., Standardized Assays for Determining the Catalytic Activity and Kinetics of Peroxidase-like Nanozymes. *Nat. Protocols* **2018**, *13* (7), 1506-1520.
- 25. Fan, W.; Lin, H.; Yuan, X.; Dai, F.; Xiao, Z.; Zhang, L.; Luo, L.; Wang, R., Expanded Porous Metal—Organic Frameworks by SCSC: Organic Building Units Modifying and Enhanced Gas-Adsorption Properties. *Inorganic Chem.* **2016**, *55* (13), 6420-6425.

- 26. Zhang, X.; Frey, B. L.; Chen, Y.-S.; Zhang, J., Topology-Guided Stepwise Insertion of Three Secondary Linkers in Zirconium Metal–Organic Frameworks. *J. Am. Chem. Soc.* **2018**, *140* (24), 7710-7715.
- 27. Fan, W.; Zhang, X.; Kang, Z.; Liu, X.; Sun, D., Isoreticular Chemistry within Metal-Organic Frameworks for Gas Storage and Separation. *Coordination Chem. Rev.* **2021**, *443*, 213968.
- 28. Bhattacharjee, S., DLS and Zeta potential What They Are and What They Are Not? *J. Control Release* **2016**, 235, 337-351.
- 29. Zhai, Q.-G.; Bu, X.; Mao, C.; Zhao, X.; Daemen, L.; Cheng, Y.; Ramirez-Cuesta, A. J.; Feng, P., An Ultra-Tunable Platform for Molecular Engineering of High-Performance Crystalline Porous Materials. *Nat. Comm.* **2016**, 7, 13645.
- 30. Yang, H.; Yang, R.; Zhang, P.; Qin, Y.; Chen, T.; Ye, F. J. M. A., A Bimetallic (Co/2Fe) Metal-Organic Framework with Oxidase and Peroxidase Mimicking Activity for Colorimetric Detection of Hydrogen Peroxide. *Microchim. Acta* **2017**, *184* (12), 4629-4635.
- 31. Sarkisov, L.; Martin, R. L.; Haranczyk, M.; Smit, B., On the Flexibility of Metal-Organic Frameworks. *J. Am. Chem. Soc.* 2014, 136 (6), 2228-2231.
- 32. Surblé, S.; Serre, C.; Mellot-Draznieks, C.; Millange, F.; Férey, G., A New Isoreticular Class of Metal-Organic-Frameworks with the MIL-88 Topology. *Chem. Commun.* 2006, (3), 284-286.
- 33. Ramsahye, N. A.; Trung, T. K.; Scott, L.; Nouar, F.; Devic, T.; Horcajada, P.; Magnier, E.; David, O.; Serre, C.; Trens, P., Impact of the Flexible Character of MIL-88 Iron(III) Dicarboxylates on the Adsorption of n-Alkanes. *Chem. Mater.* 2013, 25 (3), 479-488.
- 34. Lind, J.; Merenyi, G.; Eriksen, T. E. Chemiluminescence Mechanism of Cyclic Hydrazides such as Luminol in Aqueous Solutions. *J. Am. Chem. Soc.* **1983**, 105, 7655–7661.
- Ivanova I. P.; Trofimova, S. V.; Piskarev, I. M.; Aristova, N. A.; Burhina, O. E.; Soshnikova, O. O., Mechanism of Chemiluminescence in Fenton Reaction. *J Biophys Chem.* **2012**, 3, 88–100.
- 36. Yue, L.; Liu, Y.-T., Mechanistic Insight Into pH-Dependent Luminol Chemiluminescence in Aqueous Solution. *J. Phys. Chem. B* **2020**, *124* (35), 7682-7693.
- 37. Dang, P.; Liu, X.; Ju, H.; Wu, J., Intensive and Persistent Chemiluminescence System Based on Nano-/Bioenzymes with Local Tandem Catalysis and Surface Diffusion. *Anal. Chem.* **2020,** *92* (7), 5517-5523.
- 38. Xiao, Z.; Wang, Y.; Xu, B.; Du, S.; Fan, W.; Cao, D.; Deng, Y.; Zhang, L.; Wang, L.; Sun, D., An Integrated Chemiluminescence Microreactor for Ultrastrong and Long-Lasting Light Emission. *Adv. Sci.* **2020,** *7* (15), 2000065.
- 39. Sun, X.; Lei, J.; Jin, Y.; Li, B., Long-Lasting and Intense Chemiluminescence of Luminol Triggered by Oxidized g-C3N4 Nanosheets. *Anal. Chem.* **2020**, *92* (17), 11860-11868.
- 40. Chen, X.; Wang, X.; Fang, Y.; Zhang, L.; Zhao, M.; Liu, Y., Long-Lasting Chemiluminescence-Based POCT for Portable and Visual Pathogenic Detection and In Situ Inactivation. *Anal. Chem.* **2022**.
- 41. Moldovan, Z.; Popa, D. E.; David, I. G.; Buleandra, M.; Badea, I. A., A Derivative Spectrometric Method for Hydroquinone Determination in the Presence of Kojic Acid, Glycolic Acid, and Ascorbic Acid. *J. Spectroscopy* **2017**, *2017*.
- 42. Ciucu, A.; Patroescu, C. J. A. l., Fast Spectrometric Method of Determining the Activity of Glucose Oxidase. *Anal. Lett.* **1984**, *17* (12), 1417-1427.
- 43. Tian, F.; Zhang, S.; Liu, C.; Han, Z.; Liu, Y.; Deng, J.; Li, Y.; Wu, X.; Cai, L.; Qin, L., Protein Analysis of Extracellular Vesicles to Monitor and Predict Therapeutic Response in Metastatic Breast Cancer. *Nature Comm.* **2021**, *12* (1), 1-13.
- 44. Sun, N.; Lee, Y.-T.; Zhang, R. Y.; Kao, R.; Teng, P.-C.; Yang, Y.; Yang, P.; Wang, J. J.; Smalley, M.; Chen, P.-J., *et. al* Purification of HCC-Specific Extracellular Vesicles on Nanosubstrates for Early HCC Detection by Digital Scoring. *Nature Comm.* **2020**, *11* (1), 1-12.

# **Supporting Information**

# Highly Stable Fe/Co-TPY-MIL-88(NH<sub>2</sub>) Metal-Organic Framework (MOF) in Enzymatic Cascade Reactions for Chemiluminescence-based Detection of Extracellular Vesicles

Qiaoshi Jiang,¹ Yuchen Xiao,² Anh N. Hong,² Yuyang Shen,¹ Zongbo Li,² Pingyun Feng², \* and Wenwan Zhong¹,²,\*

<sup>1</sup>Environmental Toxicology Graduate Program; <sup>2</sup>Department of Chemistry, University of California-Riverside, Riverside, CA 92521, U.S.A.

# **Corresponding Author**

\* E-mail: pingyun.feng@ucr.edu; wenwan.zhong@ucr.edu

# **Table of Contents**

| 1.  | Illustration of pore space partition                    | S-2  |
|-----|---|------|
| 2.  | Material characterization.                              | S-3  |
| 3.  | Catalytic activity evaluation.                          | S-7  |
| 4.  | CL generation by enzyme cascades                        | S-10 |
| 5.  | Detection of GOx based on CL system                     | S-12 |
| 6.  | Aptamer conjugation and detection comparison with ELISA | S-13 |
| 7.  | Ion releasing study by ICP-OES                          | S-16 |
| Ref | ference   | S-16 |

# 1. Illustration of pore space partition

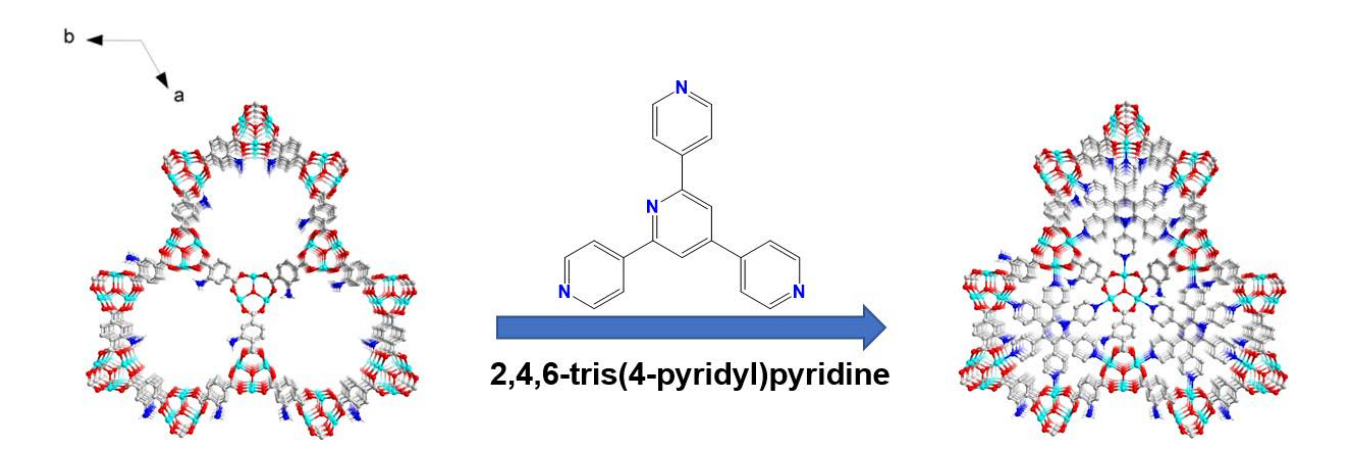


Figure S1. Illustration of pore space partition through symmetry matching regulated ligand insertion, viewed along c axis.

# 2. Material characterization.

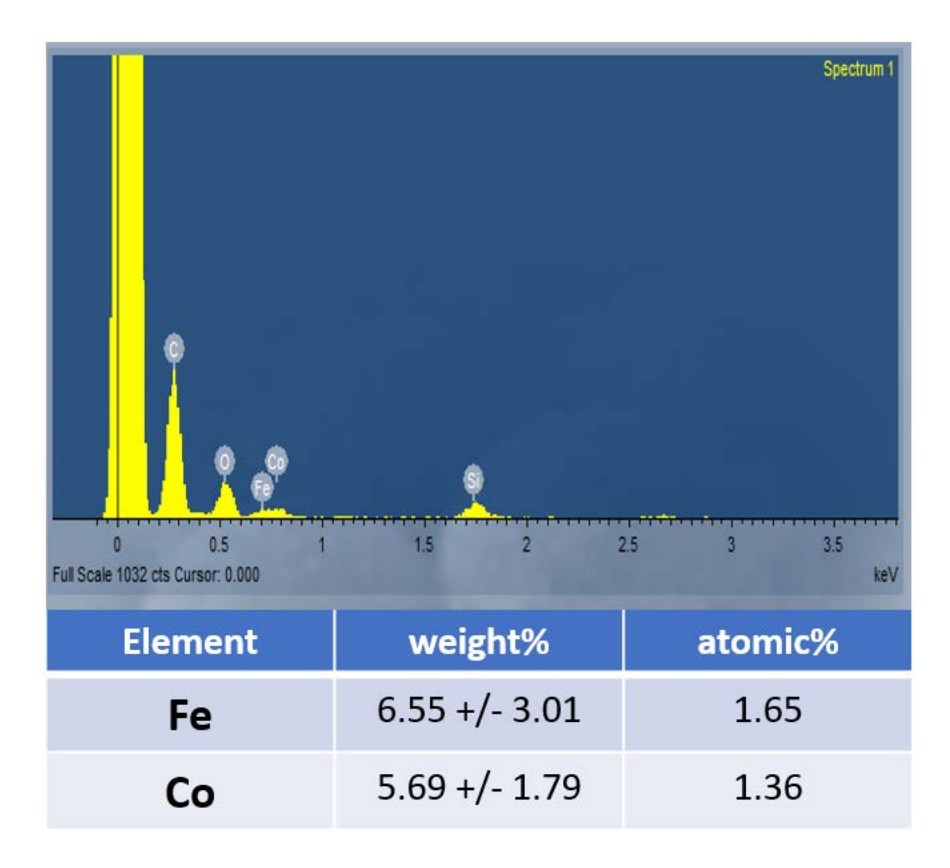


Figure S2. EDS scanning spectra of activated Fe/Co-TPY-MIL-88(NH<sub>2</sub>).

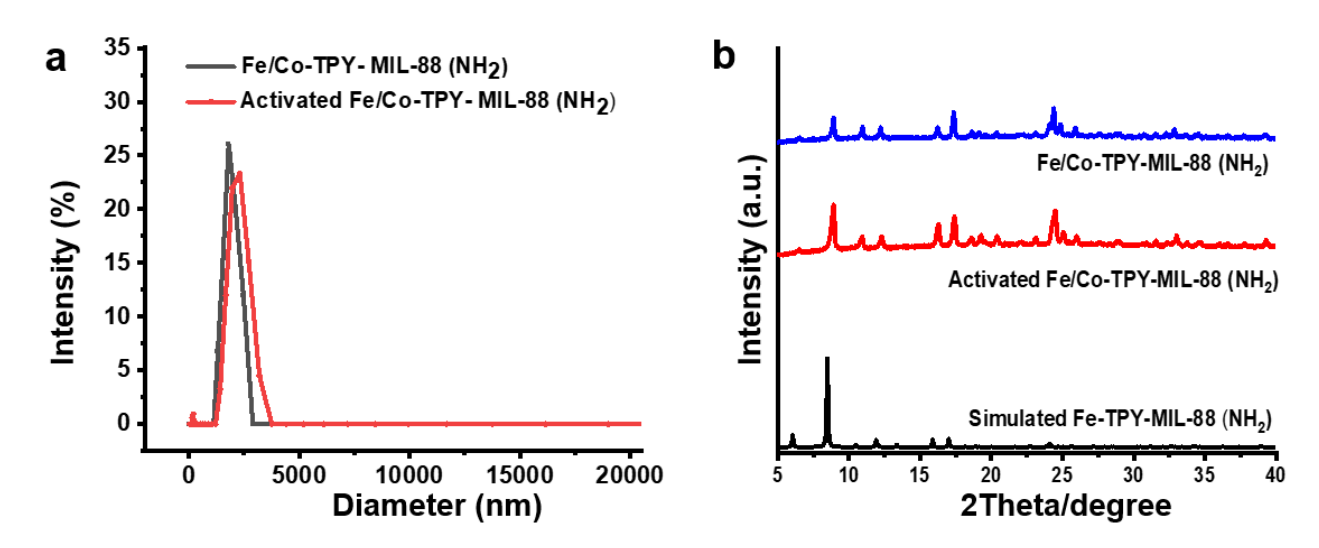


Figure S3. a) Dynamic Light Scattering results and; b) Powder X-ray diffraction patterns for Fe/Co-TPY- MIL-88(NH<sub>2</sub>) before and after activation; The simulated Fe-TPY-Mil-88(NH)<sub>2</sub> shown in b) was reprinted from Wei, Y.-S.; Zhang, M.; Kitta, M.; Liu, Z.; Horike, S.; Xu, Q., J. Am. Chem. Soc. 2019, 141, 7906-7916 (Ref. 23 in main text). Copyright 2019 American Chemical Society. The Powder X-ray diffraction experiments were performed on a PANalytical Empyrean Series 2 diffractometer, which was operating at 45 kV and 40 mA (Cu Kα radiation,  $\lambda$  = 1.5418 Å). The data collection was performed at room temperature in the range from 5° to 40° with a step size of ~0.026°.

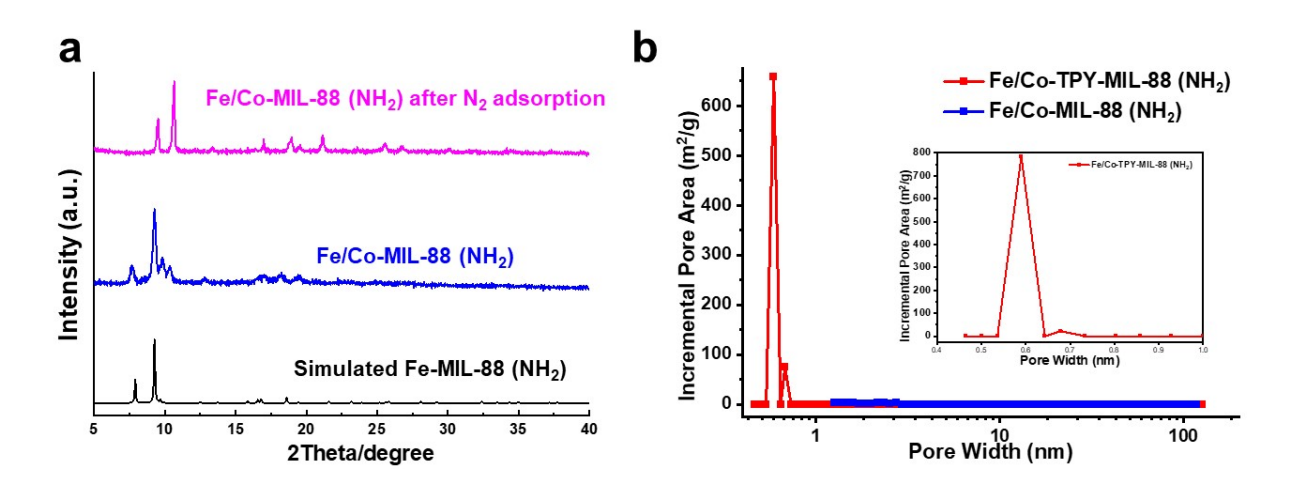
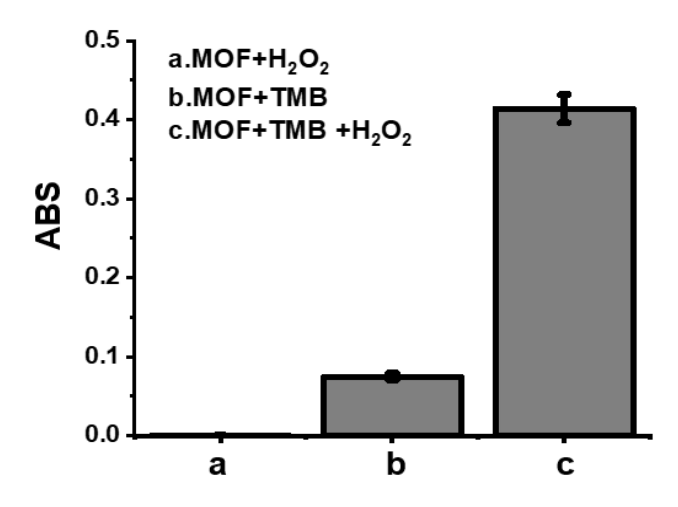


Figure S4. a) The PXRD patterns of Fe/Co-MIL-88(NH<sub>2</sub>) (synthesized by condition 2, assynthesized and after N<sub>2</sub> adsorption). b) The DFT (Density Functional Theory) pore size distribution of Fe/Co-TPY-MIL-88(NH2) and Fe/Co-MIL-88(NH2) obtained from N2 adsorptions at 77 K. The pore width of Fe/Co-TPY-MIL-88(NH2) has a peak concentrate at 0.590 nm, and Fe/Co-MIL-88(NH2) nearly has no pores. For only inset Fe/Co-TPY-MIL-**88(NH<sub>2</sub>)** DFT pore size distribution, the pressure range of  $P/P_0 < 10^{-3}$  was applied to calculate the pore size due to the micro-porous feature of this family of materials. The Fe/Co-MIL-88(NH<sub>2</sub>) MOF materials were prepared via the solvothermal method with slight adjustment from what we reported before (condition 2). In a typical approach, 0.042 g FeCl<sub>3</sub> · 6H<sub>2</sub>O, 0.043 g Co(NO<sub>3</sub>)<sub>2</sub> · 6H<sub>2</sub>O, and 0.056 g H<sub>2</sub>(NH<sub>2</sub>)BDC were dissolved in 4.029 g DMA and 2.019 g DMPU in a 23-mL glass bottle, then added 3 small drops of HFP, stirred for ~30 min, and then heated in 140 °C for 24 hours. After being cooled to room temperature, the brown-color crystal Fe/Co-MIL-88(NH<sub>2</sub>) was washed with DMA, collected by centrifugation, and dried at room temperature. MOF crystals were washed twice with ethanol at room temperature and then dried by vacuum to remove the residual solvents. Both condition 1 and condition 2 lead to the synthesis of Fe/Co-MIL-88(NH2) MOF materials. The PXRD collection condition was described in the Experimental section of the main text. The simulated Fe-Mil-88(NH)<sub>2</sub> shown in a) was reprinted from Wei, Y.-S.; Zhang, M.; Kitta, M.; Liu, Z.; Horike, S.; Xu, Q., J. Am. Chem. Soc. **2019**, 141, 7906-7916 (Ref. 23 in main text). Copyright 2019 American Chemical Society.

| MOF                                    | Average Size (nm) | Zeta Potential (mV)<br>in water | Zeta Potential (mV)<br>in buffer |
|--|-------------------|---------------------------------|----------------------------------|
| Fe/Co-TPY-MIL-88<br>(NH <sub>2</sub> ) | $1800 \pm 50$     | $7.13 \pm 0.37$                 | 14.91 ± 4.81                     |
| Fe/Co-MIL-88 (NH <sub>2</sub> )        | 699 ± 101         | $26.10 \pm 0.10$                | $18.58 \pm 0.85$                 |

**Table S1.** Dynamic Light Scattering (DLS) and Zeta Potential measurement results of the activated Fe/Co-TPY-MIL-88(NH<sub>2</sub>) and Fe/Co- MIL-88(NH<sub>2</sub>). Material suspension was prepared at 0.1 mg/mL. DLS was carried out in distilled water, and zeta-potential measurement was done in water or in the enzyme reaction buffer, 200 mM HAc-NaAc solution at pH 4.1.

# 3. Catalytic activity evaluation.



*Figure S5.* Light absorbance (ABS) at 652 nm of the 100- $\mu$ L reaction mixture of 1.0 mM TMB, 1.0 mM H<sub>2</sub>O<sub>2</sub>, and 50  $\mu$ g/mL MOF, and the two control reactions that mixed the MOF with TMB or H<sub>2</sub>O<sub>2</sub> only. All reactions measured at 15 min.

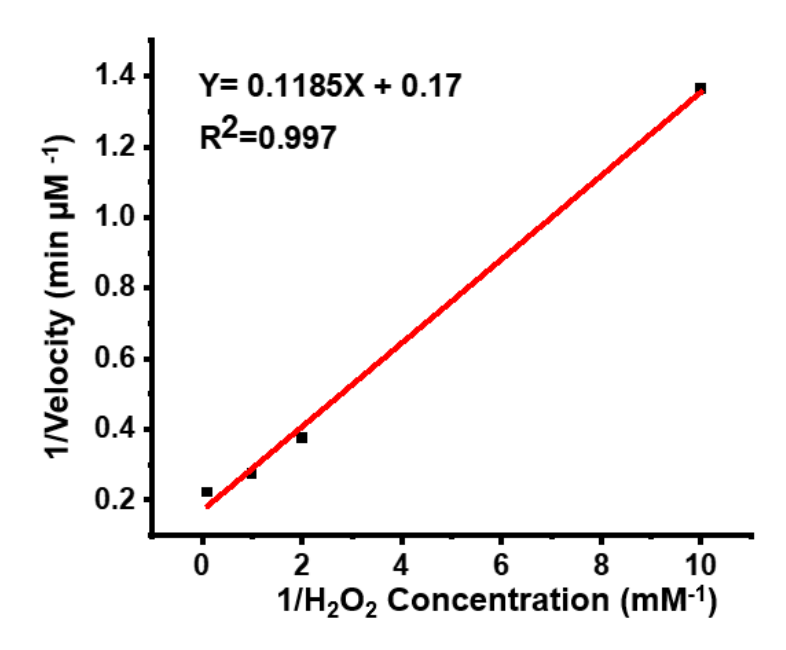


*Figure S6.* The double reciprocal of Michaelis–Menten fitting curve that plots the initial velocities within the first 15 min against  $H_2O_2$  concentrations. Reaction conditions: TMB = 1 mM, Fe/Co-TPY-MIL-88(NH<sub>2</sub>) = 50  $\mu$ g/mL, 200 mM NaAc-HAc buffer at pH 4.1.

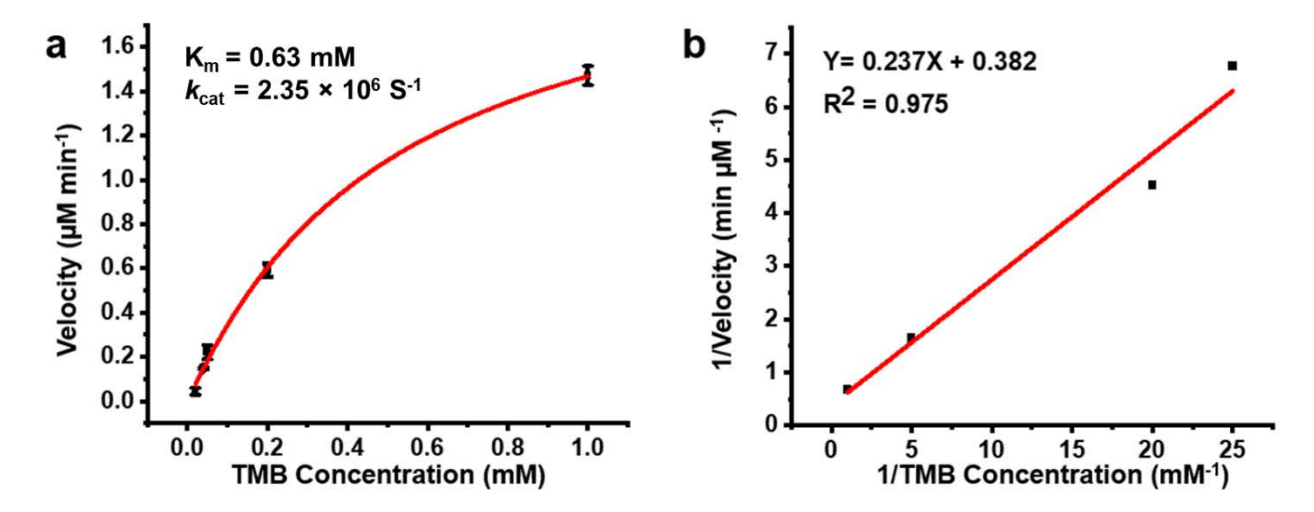


Figure S7. Steady-state kinetics study of Fe/Co-TPY-MIL-88(NH<sub>2</sub>). a) The Michaelis–Menten curve that plots the initial •OH generation velocities within the first 15 min against TMB concentrations. b) The double reciprocal of Michaelis–Menten fitting curve using data shown in a). Reaction conditions:  $H_2O_2 = 0.2$  mM, Fe/Co-TPY-MIL-88(NH<sub>2</sub>) = 50 µg/mL, 200 mM NaAc-HAc buffer at pH 4.1.

## 4. CL generation by enzyme cascade.

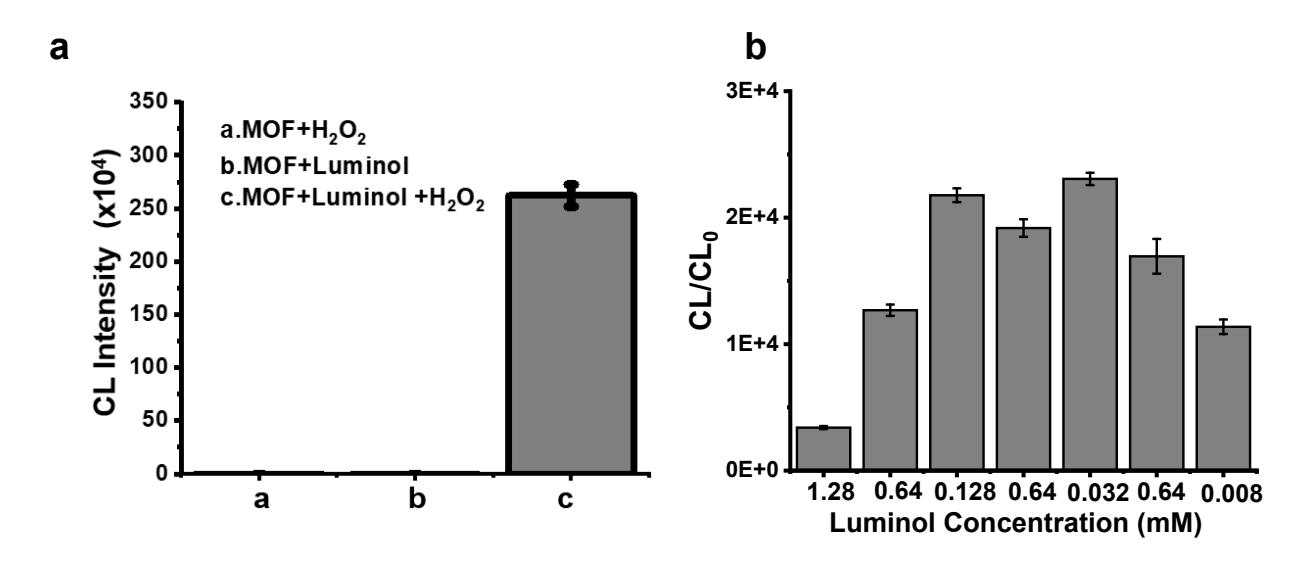
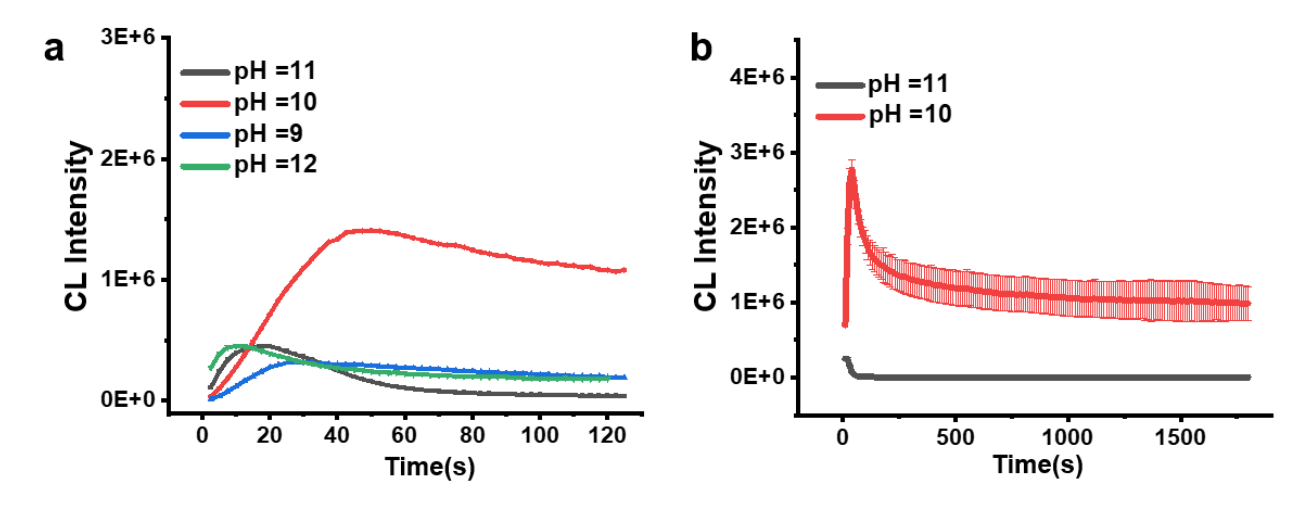


Figure S8. a) Chemiluminescence (CL) of the 100-μL mixture of 1.0 mM  $H_2O_2$ , 0.002 mM Luminol, and 50 μg/mL MOF in 10 mM borate buffer (pH 10.0) and the two control reactions of mixing the MOF with luminol or  $H_2O_2$  only. b) Optimization of the luminol concentrations in the luminol/ $H_2O_2$ /MOF chemiluminescence system that contains 1 mM  $H_2O_2$  and 50 μg/mL MOF in 10 mM borate buffer (pH 10.0). CL and CL<sub>0</sub> were the signals measured with and without  $H_2O_2$  added, respectively.



*Figure S9.* CL generation by the MOF/GOx/luminol/glucose systems at different pH monitored for a) 120 seconds (one time measurement), The buffers delivered different pH values: 10mM borate buffer (pH 9.0 & 10.0), NaOH solution (pH 11.0 & 12.0); and b) 1,800 seconds (error bars representing 3 repeated measurements). Reaction conditions: glucose = 1 mM, luminol = 0.032 mM, 25  $\mu$ g/mL MOF, 250  $\mu$ g/mL GOx,10 mM borate buffer (pH 10.0) or NaOH solution (pH 11.0).

# 5. Detection of GOx based on CL system.

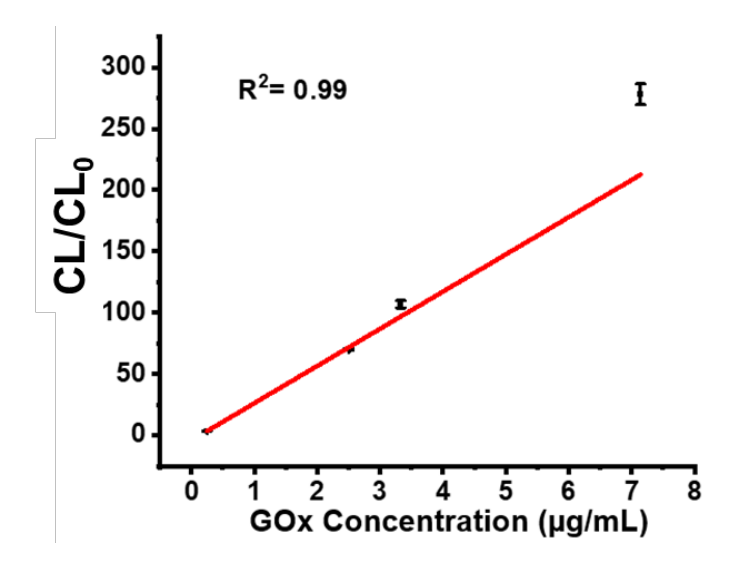
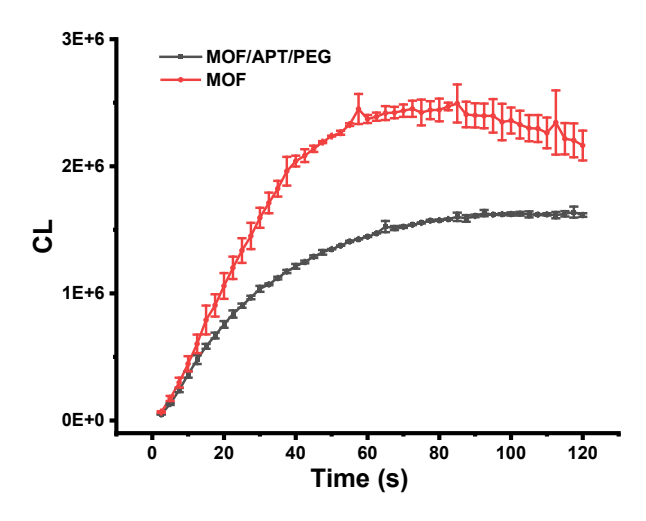


Figure S10. GOx determination based on the CL produced by the MOF/GOx/luminol/glucose system. Detection conditions: Glucose = 1 mM, luminol = 0.032 mM, MOF = 25  $\mu$ g/mL, GOx = 7.14  $\mu$ g /mL-0.25  $\mu$ g/mL, 10 mM borate buffer (pH 10.0). CL and CL<sub>0</sub> were the chemiluminescence signals measured with and without GOx added, respectively.



*Figure S11*. Impact of bioconjugation to the peroxidase-mimicking activity of the MOF. Reaction conditions: 1 mM glucose, luminol= 0.032mM, MOF=17.5 mg/ml (before and after aptamer/PEG conjugation as described in Experimental section), 0.25 mg/ml GOx, in 10 mM borate buffer (pH 10.0)

## 6. Aptamer conjugation and detection comparison with ELISA

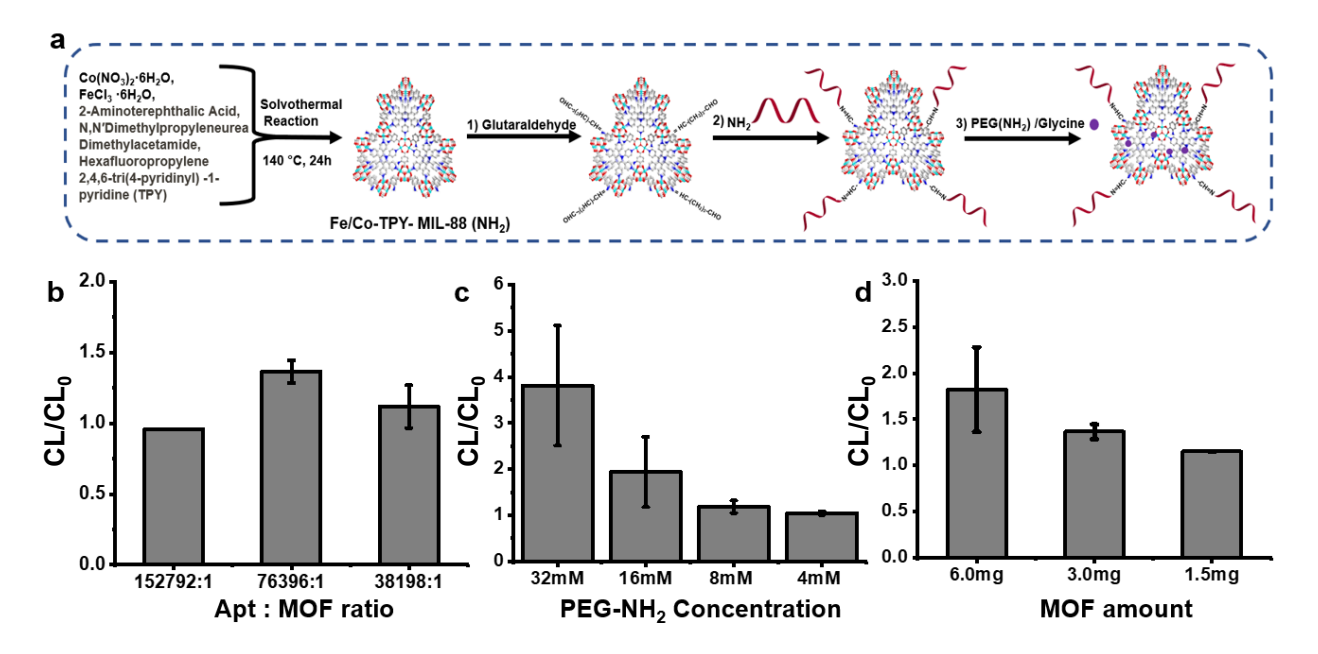
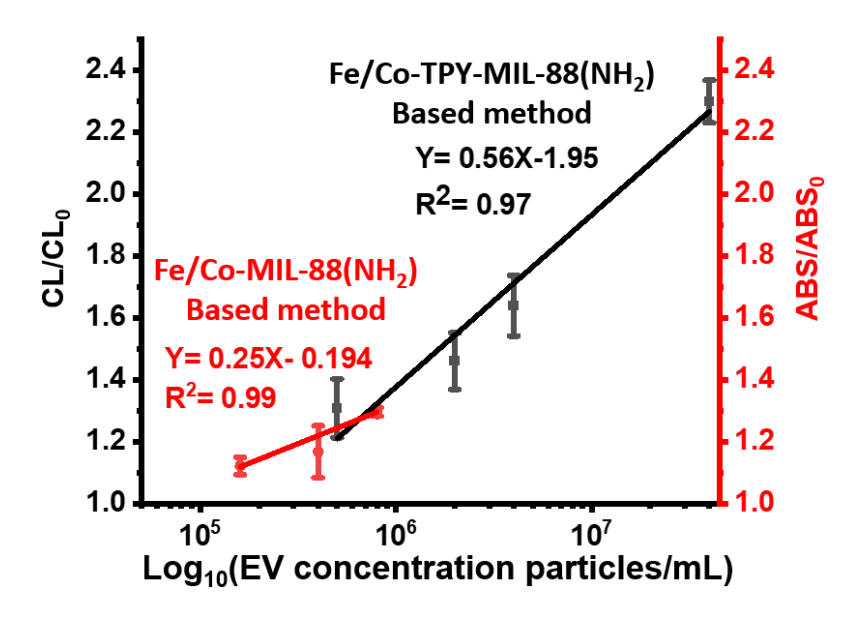


Figure S12. a) The preparation process of Fe/Co-TPY-MIL88(NH<sub>2</sub>)/CD63/PEG(NH<sub>2</sub>) bioconjugates. Optimization of conjugation conditions, focusing on b) the molar ratio of Apt: MOF; c) the concentration of PEG-NH<sub>2</sub> used. d) The amount of MOF used for EV detection. EV concentration:  $4 \times 10^6$  particles/mL; detection solution:1 mM glucose, 0.032 mM luminol, in 10 mM borate buffer (pH 10.0). CL and CL<sub>0</sub> were the chemiluminescence signals measured with and without EV added, respectively.



**Figure S13**. Comparison of signal changes obtained at various EV concentrations using the Fe/Co-TPY-MIL-88(NH<sub>2</sub>) MOF and the Fe/Co-MIL-88(NH<sub>2</sub>) MOF for enzymatic cascade reaction. Calibration curves for detection of EVs dispersed in 1× PBS. EVs were captured by 3.0 mg anti-CD63 aptamer-conjugated MOF and bound to the biotinylated anti-CD9 (black curve). The signal from the former MOF is CL, and that from the latter MOF is absorbance at 652 nm. Detection solution:1 mM glucose, 0.032 mM luminol, in 10 mM borate buffer (pH 10.0) for CL; The detection solution contained 0.50 mM TMB, and 0.50 mM glucose, in 200 mM NaAc–HAc buffer at pH 4.1 for ABS. CL and CL<sub>0</sub> were the chemiluminescence measured with and without EV added, respectively. ABS and ABS<sub>0</sub> were the absorbance measured with and without EV added, respectively.

# 7. Ion releasing study by ICP-OES

| Treatment  | Cobalt% released per unit<br>mass of Co in MOF | Iron% released per unit mass<br>of Fe in MOF |
|--|--|--|
| Fe/Co-TPY-MIL-88(NH <sub>2</sub> ) MOF incubated at pH 12            | 12%  | 29%  |
| Fe/Co-TPY-MIL-88(NH <sub>2</sub> ) MOF incubated at pH 10            | 5.0%   | 11%  |
| Fe/Co-TPY-MIL-88(NH <sub>2</sub> ) MOF incubated at pH 7             | 5.0%   | 9.4%   |
| Fe/Co-TPY-MIL-88(NH <sub>2</sub> ) MOF in enzymatic cascade reaction | 1.0%   | 2.2%   |
| Fe/Co-TPY-MIL-88(NH <sub>2</sub> ) MOF in serum                      | 0.51%  | 0.10%  |

*Table S2.* ICP-OES analysis of ion release from MOF at pH 12, 10, and 7 (2.5 mg MOF incubated in 12.23 mL of 10 mM phosphate buffer pH 7.0, 10 mM borate buffer pH 10.0 or NaOH solution pH 12.0 for 15 min); during cascade reaction (2.5 mg MOF suspended in 9.785 mL of 10 mM borate buffer (pH 10.0) containing 1 mM glucose, 0.032 mM luminol, and 0.25 mg GOx, for 15 min); and during incubation in serum (20 mg MOF suspended in 1 mL diluted serum for 3 hrs).